High-Affinity Actin-Binding Nebulin Fragments Influence the ActoS1 Complex†

Douglas D. Root‡,§ and Kuan Wang*,‡,||

Department of Chemistry and Biochemistry, University of Texas at Austin, Austin, Texas 78712, Department of Biological Sciences, University of North Texas, P.O. Box 305220, Denton, Texas 76203-5220, and Laboratory of Physical Biology, National Institute of Arthritis and Musculoskeletal and Skin Diseases, National Institutes of Health, Bethesda, Maryland 20892

Received June 30, 2000; Revised Manuscript Received October 17, 2000

ABSTRACT: Human nebulin fragments, NA3 and NA4, corresponding to individual superrepeats display high-affinity interactions with individual actin protomers in cosedimentation and solid-phase binding assays. Stoichiometric analysis of nebulin fragment-induced actin polymerization and inhibition of actin-activated S1 ATPase indicate that one superrepeat influences multiple actin molecules along the F-actin filament, consistent with a combination of strong and weak interactions of nebulin over the length of the actin filament. The mechanisms by which human nebulin fragments affect the interaction between actin and myosin S1 are studied by fluorescence quenching, polarization, and resonance energy transfer. We show that, under strong binding conditions, premixing actin with the NA3 prior to adding myosin subfragment 1 (S1) inhibits the rate of actoS1 association. The nebulin fragments, NA3 and NA4, caused little effect on the extent of actoS1 binding at equilibrium but did alter the nature of the complex as evidenced by an increase in the resonance energy transfer efficiencies between S1 and actin in the absence of ATP. The addition of low concentrations of ATP rapidly dissociates the strong-binding actoS1 irrespective of the presence or absence of nebulin fragment. Interestingly, the strongly bound state reforms rapidly after S1 hydrolyzes all available ATP. These observations are consistent with the notion that nebulin might contribute to optimizing the alignment of actomyosin interactions and inhibit suboptimal actomyosin contacts.

Nebulin comprises 2−3% of the myofibrillar protein of skeletal muscle and displays tissue and development specific isoforms, with a size ranging from 600 to 900 kDa in a variety of muscle types (*1*−*4*). Immunoelectron microscopy suggests that a single nebulin molecule spans the whole length of a thin filament with its C-terminus anchored at the Z-line and it accompanies the actin filament during muscle contraction (*2*, *3*, *5*−*8*). These data suggest that nebulin forms a composite filament with actin/tropomyosin/troponin, perhaps by binding laterally to actin in situ. Significantly, the sizes of nebulin isoforms are proportional to the length of the thin filaments in many skeletal muscles (*3*, *4*). These correlations strongly suggest that nebulin may act as a protein ruler that regulates the length of thin filaments.

Analysis of deduced protein sequence and structural motifs of skeletal muscle nebulins reveals the design principles of this giant multifunctional protein in the sarcomere. The bulk of nebulin is constructed of about 200 tandem copies of an approximately 35-residue module. These modules can be classified into seven types. The majority of the nebulin modules form 22 superrepeats, with each superrepeat containing a seven-module set (one of each type in the same order). These superrepeats are further grouped into large segments: at least six segments contain adjacent, homologous superrepeats, and one segment contains eight nebulin modules of the same type. Differential splicing in the superrepeat region generates nebulin size isoforms (*9*−*11*). The long string of nebulin modules is bracketed by a unique N-terminal domain and a C-terminus containing a linker sequence and a Src-homology domain 3 (SH3). Both the linker and SH3 are implicated in the targeting of nebulin to the Z line (*9*, *10*, *12*−*15*). This four-domain layout appears to be shared by the smaller isoform, nebulette, found exclusively in cardiac muscle cells (*12*−*14*).

Actin-binding studies with recombinant nebulin fragments containing 2−15 modules, small native nebulin fragments,

† D.D.R. was supported in part by a MDA Postdoctoral Fellowship. This work was supported by in part by grants from NIH (AR43512 to K.W. and AR44737 to D.D.R.).

* Address correspondence to this author at the NIH. Phone: (301)-496-4097. Fax: (301)402-8566. E-mail: wangk@exchange.nih.gov.

‡ University of Texas at Austin.

§ University of North Texas.

|| National Institutes of Health.

[1] Abbreviations: A, actin; *a*/*b*, axial ratio; B, bound concentration; BrAEDANS, 5-((((2-bromoacetyl)amino)ethyl)amino)naphthalene-1-sulfonic acid; *C*, concentration; $<d_A^x>$ and $<d_D^x>$, fluorescence depolarizations of acceptor and donor, respectively; $D_{w,20}$, diffusion constant; DABMI, 4-dimethylaminophenylazophenyl-4-maleimide; DTT, dithiothreitol; *E*, efficiency of energy transfer; ϵ_A, extinction coefficient of the acceptor; *F*, fluorescence intensity; *f*, frictional coefficient; FRET, fluorescence resonance energy transfer; IAF, iodoacetamidofluorescein; IAEDANS, 5-((((2-iodoacetyl)amino)ethyl)amino)naphthalene-1-sulfonic acid; IANBD, *N*-(2-(iodoacetoxyethyl)-*N*-methyl)amino-7-nitrobenz-2-oxa-1,3-diazole; *J*, overlap integral; *K*, dissociation constant; *k*, rate constant; K, unidirectional rotational constant; κ^2, orientation factor; k_B, Boltzman's constant; *M*, molecular mass; MIANS, 2-(4-maleimidylanilino)naphthalene-6-sulfonic acid; *N*, nebulin fragment concentration; η, refractive index; N_o, Avogadro's number; NA3, an 8-module nebulin fragment; NA4, a 7-module nebulin fragment; *P*, polarization of fluorescence; ρ, density; Q_D, quantum yield of the donor; QS, quinine sulfate; *R*, separation distance; R_o, critical transfer distance; R_v and R_h, ratios of vertically to horizontally polarized fluorescent emissions from vertically or horizontally polarized light, respectively; r^2, correlation coefficient; *S*, S1 concentration; *r*, radius; S1, myosin subfragment 1; τ, fluorescence lifetime; *V*, partial specific volume; *V*(*r*), volume as a function of tube radius; ω, angular velocity.

10.1021/bi0015010 CCC: $20.00
Published on Web 01/11/2001

and synthetic peptides (*7*, *16*−*18*, *21*−*23*) indicate that the 35-residue repeat is the basic structural unit of the actin binding domains in nebulin. If all sites are operative in situ, then nebulin may contain a string of about 200 actin-binding domains along its length and would act as a zipper in its lateral association with actin (*24*). A one to one matching between nebulin modules with actin protomers would allow nebulin to operate as a protein ruler to determine or stabilize the length of actin filaments (*3*, *4*, *9*, *19*).

Recent studies of the effect of nebulin fragments on actin−myosin interaction and its regulation by calmodulin raise the intriguing possibility that nebulin might have regulatory functions (*25*). Nebulin fragments bind with high affinity to actin and the myosin head. Fragments from the N-terminal half of nebulin that are situated in the actomyosin overlap region of the sarcomere inhibit actomyosin ATPase activities as well as sliding velocities of actin over myosin during in vitro motility assays; while a nebulin fragment near the C-terminus, which is localized to the Z-line, does not prevent actin sliding. Significantly, calmodulin reverses the inhibition of ATPase and accelerates actin sliding in a calcium-dependent manner. Calmodulin with calcium greatly reduces the binding of nebulin fragments to both actin and myosin. The data suggest that the nebulin−calmodulin system is reminiscent of caldesmon and calponin in smooth muscles (reviewed in ref *26*) and may function as a calcium-linked regulatory system that is distinct from tropomyosin/troponin on the actin filaments of skeletal muscles. Nebulin may hold myosin heads close to actin in an orientation that prevents random interaction in resting muscles yet facilitates cross-bridge cycling upon activation by calcium and calmodulin.

This hypothesis suggests that nebulin fragments may influence the interactions between actin and myosin heads and is investigated in the present study by measurements of fluorescently labeled actin and/or myosin head. NA3, an 8-module human nebulin fragment situated in the overlap region of the sarcomere, has been shown to bind both actin and S1 and inhibits actin-activated S1 ATPase and actin sliding over myosin (*25*). We show that NA3 and homologous NA4 bind both S1 and actin and induce profound changes in the actoS1 binding interaction.

EXPERIMENTAL PROCEDURES

Protein Purification. Rabbit skeletal actin was prepared according to Spudich and Watt (*27*). Rabbit skeletal myosin was prepared by the method of Godfrey and Harrington (*28*) and digested with α-chymotrypsin to S1. Human nebulin fragments, NA3 and NA4, were purified from host *Escherichia coli* as previously described (*7*, *20*, *25*). Briefly, isolated inclusion bodies were dissolved in 6 M urea, 1 mM EDTA, and 10 mM imidazole (pH 7.0) and separated on a CM52 ion-exchange column equilibrated in the same buffer and eluted with a 0−0.5 M NaCl gradient. The resulting fractions were dialyzed overnight at 4 °C against 1 mM $CaCl_2$ and 10 mM imidazole (pH 7.0) and centrifuged at 100000*g* to remove any aggregates prior to use. As described previously, dialysis to near millimolar concentrations of calcium increased the solubility of nebulin fragments in the absence of urea (*25*).

Protein concentrations were determined spectrophotometrically. The extinction coefficients ($A^{1\%}_{280nm}$) and molecular masses (Da), respectively, used were as follows: S-1, 7.5 cm^{-1}, 110 000 (*29*); actin, 11.0 cm^{-1}, 42 000 (*30*); NA3, 13.2 cm^{-1}, 31 419; and NA4, 13.4 cm^{-1}, 27 945. The extinction coefficient ($A^{1\%}_{280nm}$) of NA3 and NA4 was calculated according to Gill and von Hippel (*31*).

Fluorescent Labeling. Actin was labeled specifically on cysteine 374 with *N*-((2-(iodoacetoxy)ethyl)-*N*-methyl)amino-7-nitrobenz-2-oxa-1,3-diazole (IANBD, Molecular Probes, Eugene, OR) or *N*-(1-pyrene)iodoacetamide (Molecular Probes) by standard methods (*32*, *33*). Briefly, actin was polymerized at 2 mg/mL in G-buffer (0.1 mM $CaCl_2$, 0.2 mM ATP, 0.5 mM β-mercaptoethanol, 2 mM Tris-HCl, pH 7.6) by the addition of 2 mM $MgCl_2$ for 1 h and then incubated for 16 h at 23 °C with 0.33 mM of either IANBD or *N*-(1-pyrene)iodoacetamide. The F-actin was pelleted at 100000*g* for 1 h at 4 °C and was homogenized in G-buffer and dialyzed against the same for 2 days at 4 °C. A final ultracentrifugation at 100000*g* for 2 h removed minor amounts of aggregated material. The extent of IANBD incorporated, as determined from absorbance at 472 nm with an extinction coefficient of 23 000 M^{-1} cm^{-1}, corresponded to a 1:1 conjugate of 74% of the actin. The fraction of actin modified by pyrene iodoacetamide in different preparations ranged from 50% to 70%, as determined spectrophotometrically using an extinction coefficient of 22 000 M^{-1} cm^{-1} at 344 nm for pyrene-labeled G-actin (*32*). To ensure native conditions, the F-actin for binding assays was formed by diluting G-actin into the assay buffer without removing micromolar concentrations of residual ADP from the G-buffer.

S1 was labeled specifically on SH1 (cysteine 707) by 5-((((2-iodoacetyl)amino)ethyl)amino)naphthalene-1-sulfonic acid (IAEDANS, Molecular Probes) as reported in ref *34*. For fluorescence resonance energy transfer experiments, S1 (21 μM) in 40 mM KCl and 10 mM imidazole (pH 7.0) was incubated for 3 h at 4 °C with 10 μM IAEDANS. The addition of 1 mM DTT terminated the reaction, and subsequent dialysis at 4 °C into the experimental buffer removed any excess reagent. A specific incorporation of IAEDANS into SH1 was indicated by a decrease of K^+-EDTA ATPase activity by 8% and an elevation of calcium ATPase activity by 58% relative to unlabeled S1. The amount of IAEDANS incorporated into S1 was too low to be estimated accurately by absorption. Instead, the quantum yield of fluorescence of labeled S1 when excited at 336 nm was measured relative to the known quantum yield of quinine sulfate (in 0.1 N sulfuric acid) of 0.70 (*35*) and compared to literature values of IAEDANS-labeled S1 (0.52 ± 0.01) (*34*) by the following equation:

$$\% \text{ IAEDANS S1} = (100\, F_{S1}[QS] \times 0.70)/(F_{QS}[S1] \times 0.52) \quad (1)$$

in which F_{S1} is the total fluorescence intensity of IAEDANS-labeled S1 at a concentration of [S1], and F_{QS} is the total fluorescence intensity of quinine sulfate at a concentration of [QS]. The amount of IAEDANS incorporated into S1 (% IAEDANS S1) was calculated to be 9 ± 1%, agreeing well with the measured 8% decrease in S1 K^+-EDTA ATPase activity. This agreement and a measured elevation of Ca^{2+} ATPase activity supported the contention that SH1 was labeled specifically. A low extent of S1 labeling was

desirable for fluorescence resonance energy transfer experiments, since it ensured that only SH1, the most reactive cysteine on S1, was modified.

For fluorescence polarization measurements of IAEDANS-labeled S1, the specificity of modification was less critical, and a higher degree of labeling was desirable. S1 (18.6 μM) in 40 mM KCl and 10 mM imidazole (pH 7.0) was incubated for 16 h at 4 °C with 44 μM IAEDANS, followed by the addition of 1 mM DTT to terminate the reaction and dialysis to remove excess reagent. The sample was dialyzed against the experimental buffer overnight at 4 °C. A 95% decrease of K^+-EDTA ATPase activity and a 50% decrease of calcium ATPase activity indicated significant incorporation of IAEDANS into myosin SH1 and SH2. In all experiments, S1 was used at low ionic strength to enhance its interactions with actin to levels that are more representative of the extent to which myosin heads interact with actin under the physiological conditions in the muscle.

Ca^{2+} and K^+-EDTA ATPase Assays. The calcium ATPases were performed in 50 mM KCl, 5 mM $CaCl_2$, and 10 mM Tris-HCl (pH 7.0), and K^+-EDTA ATPases were measured in 0.3 M KCl, 1 mM EDTA, and 10 mM Tris-HCl (pH 7.0) (*36*). S1 concentrations were fixed at 1 μM. ATPase assays were stopped by the addition of 0.1 N sulfuric acid. The phosphate released from ATP (2 mM) at 25 °C was determined by the malachite green assay (*37*).

Fluorescence Measurements of Pyrene Quenching, IAEDANS Polarization, and FRET. All measurements of fluorescence were made with an SLM 8000 spectrofluorometer (SLM Instruments, Inc., Urbana, IL) equipped with adjustable excitation and emission polarization filters. Channel ratioing to a reference cell was done to reduce error from fluctuations in lamp intensity. Samples were evaluated in 1-mL quartz cuvettes. Temperature was controlled at 25 °C in all experiments. Absorbance spectra were collected in an 8452A diode array spectrophotometer (Hewlett-Packard, Waldbronn, Germany).

The fluorescent intensity of pyrene actin after excitation at 365 nm was determined at 407 nm at 1-s intervals. Photobleaching was monitored in control experiments and did not cause significance quenching to affect rate measurements of fluorescence quenching by S1. The data in Figure 1A were fit by a simple binding isotherm as expressed by the following equation, which is based on an observed 80% quenching of pyrene actin by S1:

$$\%F = 100\% - 80\%(A + S + K - ((A + S + K)^2 - 4AS)^{0.5})/2A \quad (2)$$

In this equation, %F is the relative fluorescence intensity at 407 nm (expressed as percent of pyrene actin fluorescence in the absence of S1), A is the total actin concentration (1.7 μM), S is the total S1 concentration (0−4.0 μM), and K is the dissociation constant.

Rates of pyrene actin fluorescence quenching were well fit by the sum of two exponential decays with

$$F(t) = a \exp(-k_1 t) + b \exp(-k_2 t) - 0.2F_o \quad (3)$$

where t is time, $F(t)$ is the relative fluorescence intensity at time t, F_o is the relative fluorescence intensity in the absence of S1, k_1 and k_2 are rate constants, and a and b are constants that depend on the units of fluorescence intensity and relative contributions of the two exponentials. A correction factor $-0.2F_o$ was applied because 20% of the pyrene fluorescence remained unquenched at saturating concentrations of S1.

Table 1: Fluorescence Energy Transfer Distances (in Å)

components	$R_{2/3}$[a]	R_4
S1−A[b]	45 (43; 47)	61
S1−A−NA3	20 (17; 23)	27
S1−NA3−A	25.3 (25.1; 25.5)	34
S1−A−NA3	60 (58; 62)	80
S1−A−ATP	66 (61; 71)	90
S1−A−NA3−ATP	72 (64; 80)	96

[a] Each pair of distances in the parentheses represent values determined by exciting at 370 vs 336 nm, respectively. The experimental errors were smaller than this range. [b] Dashes indicate the order of addition S1 (0.5 μM), F-actin (abbreviated as A, 1.0 μM), NA3 (2.0 μM), ATP (2.5 μM), and premixed F-actin with NA3 (abbreviated as ANA3).

Fluorescence polarization of IAEDANS-labeled S1 after excitation at 370 nm was determined over an emission range from 410 to 610 nm at 2-nm intervals. The fluorescence polarization, P, was calculated by

$$P = (R_v - R_h)/(R_v + R_h) \quad (4)$$

in which R_v is the ratio of background-corrected vertically to horizontally polarized emissions intensities resulting from vertically polarized excitations, and R_h is the ratio of background-corrected vertically to horizontally polarized emissions intensities resulting from horizontally polarized excitations (for a review, see ref *38*). When excited at 370 nm, the peak emission intensity of IAEDANS-labeled S1 was at 483 nm, which was used for reporting the fluorescence polarization.

Fluorescence resonance energy transfer measurements were made by steady-state fluorescence methods. The quenching of donor fluorescence (IAEDANS on SH1 of S1) by acceptors (IANBD on cysteine 374 of F-actin) was performed at two excitation wavelengths to assess the possible contributions of multiple fluorescence dipoles of the donor: 336 nm (measuring emissions from 410 to 514 nm) and 370 nm (measuring emissions from 442 to 492 nm) at 2-nm intervals. The small range in measurements based on differences between exciting at 336 nm versus 370 nm is expressed parenthetically in Table 1. Emissions spectra of the donor in the presence and absence of acceptor were plotted on the same axes, and the difference in the spectra over the desired range was graphically integrated with the public domain NIH Image 1.56 program (written by Wayne Rasband at the U.S. National Institutes of Health) on a Power Macintosh 7100 computer.

The efficiency of transferring energy between singlet states of two fluorophores depends on the ensemble average distance between a donor (IAEDANS) on S1 and an acceptor (IANBD) on actin, according to (see ref *39* for a review):

$$E = R_o^6/(R^6 + R_o^6) \quad (5)$$

In this equation, E is the fractional efficiency of transfer, R_o is the critical transfer distance between the donor and acceptor at which $E = 0.5$, and R is the actual distance separating the donor and the acceptor.

The distance between the donor and the acceptor was calculated with eq 5 from the efficiency of energy transfer and estimating R_o with the following equation:

$$R_o = (8.785 \times 10^{-5} Q_D \eta^{-4} \kappa^2 J)^{1/6} \text{ Å} \quad (6)$$

The quantum yield of the donor in the absence of acceptor, Q_D, was taken to be 0.52 ± 0.01 (*34*). The refractive index, η, was 1.4. The orientation factor, κ^2, ranged from 0 to 4.

The overlap integral, J, was calculated from the spectra in Figure 3A according to

$$J = \sum_{\Delta\lambda}[F_D(\lambda)\epsilon_A(\lambda)\lambda^4\Delta\lambda]/\sum_{\Delta\lambda}[F_D(\lambda)\Delta\lambda] \quad (7)$$

The corrected donor emission spectrum, F_D, is in arbitrary units. The absorption extinction coefficient, ϵ_A, is expressed in M^{-1} cm^{-1}. The wavelength, λ, is in nm. When the donor was excited at either 336 or 370 nm, J was calculated to be the same. Because NA3 affected slightly the absorption spectrum of IANBD-labeled F-actin (Figure 3A), J has values of $8.5 \times 10^{14} \pm 0.1 \times 10^{14}$ cm^3 M^{-1} in the absence of NA3 and $5.8 \times 10^{14} \pm 0.1 \times 10^{14}$ cm^3 M^{-1} in the presence of NA3. On the basis of these constants and $\kappa^2 = {}^2/_3$, the value of R_o for actoS1 is 43.6 Å, and R_o for the actoS1−NA3 complex is 40.9 Å.

Fluorescence depolarization measurements provide evidence that the donor and acceptor are not rigidly fixed with respect to each other; therefore, the possible range of values of κ^2 can be limited (*40*). The limiting values of κ^2 were estimated as follows. The axial fluorescence depolarizations of IAEDANS attached to SH1 of S1 and IANBD-labeled cysteine 374 of actin were calculated by taking the square of the ratio of the limiting anisotropy to fundamental anisotropy. The limiting anisotropies of IANBD−actin and IAEDANS−S1 were 0.325 (at 500 nm) (*33*) and 0.290 (at 360 nm) (*41*), respectively. The fundamental anisotropies of IANBD and IAEDANS were reported to be 0.353 (at 500 nm) (*33*) and 0.328 (at 360 nm) (*42*), respectively. These values yielded axial depolarizations of 0.960, $<d_A^x>$, for the acceptor and 0.940, $<d_D^x>$, for the donor. On the basis of the equations:

$$\kappa^2_{max} = (1 + <d_D^x> + <d_A^x> + 3<d_D^x><d_A x>)^2/_3$$

$$\kappa^2_{min} = \{1 - [(<d_D^x> + <d_A^x>)/2]\}^2/_3 \quad (8)$$

limiting values of κ^2_{max} and κ^2_{min} were calculated to be 3.7 and 0.033, respectively. As shown in Table 1, the minimal value of R (often denoted R_{min}) is significantly higher when the lower limit of κ^2_{min} is raised from 0 to 0.033. However, the difference between $\kappa^2_{max} = 3.7$ and the theoretical maximum of $\kappa^2_{max} = 4$ does not substantially affect R_{max}.

Sedimentation Equilibrium. Centrifugation of nebulin fragments in a Beckman airfuge to equilibrium permitted the determination of their molecular weights from protein distribution profiles. Nebulin fragments at 0.1−0.3 mg/mL in 2 mM $MgCl_2$, 1 mM $CaCl_2$, 10 mM imidazole (pH 7.0), and 20% sucrose to stabilize proteins during rotor deceleration sedimented to equilibrium after 80 h. The deviation from equilibrium after this time was less than 2% according to calculations based on Van Holde and Baldwin (*43*). Evaporation changed the solution volume by less than 5%. A Beckman Digital Speed Readout Accessory measured the velocity at 54 000 rpm in an A110 rotor that attained an estimated temperature of 300 K during the run. Upon deceleration of the rotor and consequent reorientation of the protein gradient, fractionation of the centrifuge tube contents by a Unimetrics syringe stabilized by a Narishige micromanipulator enabled measurement of the protein distribution profile using the Bradford method of protein concentration determination as modified by Bio-Rad. Comparison of the midvolume of each fraction to available charts yields the mean centrifugal radius. The natural logarithm of the protein concentration plotted versus the square of the centrifugal radius produces a slope (d ln C/dr^2) that is proportional to the molecular weight (M_{eq}) according to

$$M_{eq} = \text{d ln } C/\text{d}r^2(2k_B N_o T/(\omega^2(1 - V\rho))) \quad (9)$$

In this equation, $k_B N_o$ is equal to the ideal gas constant (8.3×10^7 g cm^2 s^{-2} mol^{-1} K^{-1}), T is the temperature (300 K), ω is the angular velocity (5700 s^{-1}), ρ is the density of the 20% sucrose solution (1.08 g/cm^3), and V is the partial specific volume of the nebulin fragment in 20% sucrose (calculated from amino acid composition with an accuracy of ±3% as 0.739 cm^3/g for NA3 and 0.745 cm^3/g for NA4). Combined errors in the estimation of molecular weight based on determination of slope, temperature, and rotor speed are approximately ±15%.

Since equilibrium centrifugation yields weight-averaged molecular masses, the maximum fraction of multimeric complexes are calculated using a dimer−monomer equilibrium model:

$$\Delta = 100/(1 + ((4M - 2M_{eq})/(M_{eq} - M))) \quad (10)$$

In this equation, Δ is the percent dimer, M is the monomeric molecular mass, and M_{eq} is the weight-averaged molecular mass.

Sedimentation Velocity and Hydrodynamic Shape. Ultracentrifugation of nebulin fragments at 0.04−0.06 mg/mL in 2 mM $MgCl_2$, 1 mM $CaCl_2$, 10 mM imidazole (pH 7.0), and 20% sucrose at 35 000 rpm for 18 h at 20 °C in a Beckman L5-50 ultracentrifuge with a SW41 swinging bucket rotor yielded protein distribution profiles with a distinct trailing boundary. Evaporation changed the tube volume by less than 5%. Fractionation of the centrifuge tubes by pipetting off aliquots starting from the meniscus and subsequent determination of protein concentrations by the Bradford method allowed construction of the protein distribution profile. Equations that relate the volumes of aliquots to their radial position in the ultracentrifuge are as follows:

for $r \geq 14.52$ cm:

$$V(r) = 2\pi(1 - (r - 14.52)/0.68)(0.68)^3/3) - \pi(r - 14.52)^3 (\tan(\arccos((r - 14.52)/0.68))^2/3$$

for $r \leq 14.52$ cm:

$$V(r) = 0.6585 + \pi(14.52 - r)(0.68)^2 \quad (11)$$

In these equations, r is the centrifugal radius to the meniscus of a volume, $V(r)$, which remains in the centrifuge tube after

removing each aliquot. Plots of protein concentration versus the midvolume radial position of the aliquot illustrate the trailing boundary of sedimenting protein. The centrifugal radius at the midpoint of this boundary, r_b, and at the originating meniscus, r_m, combined with the time of centrifugation, t (64 800 s), and the angular velocity, ω (3665 s^{-1}), permit calculation of the sedimentation coefficient, S_o, with

$$S_o = (\ln r_b - \ln r_m)/\omega^2 t \quad (12)$$

The following equation corrects the sedimentation coefficient to dilute aqueous solution at 20 °C, $S_{a,20}$, using the partial specific volumes of the nebulin fragments V_a (0.728 cm^3/g for NA3 and 0.733 cm^3/g for NA4) in the absence and V (0.739 cm^3/g for NA3 and 0.745 cm^3/g for NA4) in the presence of 20% sucrose, the solution densities ρ_a (1.00 g/cm^3) in the absence and ρ (1.08 g/cm^3) in the presence of 20% sucrose, and the solution viscosities η_a (0.0100 P) in the absence and η (0.0195 P) in the presence of 20% sucrose:

$$S_{a,20} = S_o\eta(1 - V_a\rho_a)/(\eta_a(1 - V\rho)) \quad (13)$$

The Svedberg equation allows calculation of the diffusion constant, $D_{w,20}$:

$$D_{w,20} = S_{w,20}RT/(M(1 - V_a\rho_a)) \quad (14)$$

The frictional ratio is calculated by

$$f/f_{min} = (kT/D_{w,20})/(6\pi\eta_a(3MV_a/4\pi N_o)^{1/3}) \quad (15)$$

in which f is the observed frictional coefficient, f_{min} is the minimum possible frictional coefficient, k is Boltzmann's constant (1.38×10^{-16} g $cm^2/K\ s^2$), and N_o is Avogadro's number (6.022×10^{23} mol^{-1}).

The axial ratio of a prolate ellipsoid (a/b) is computed from

$$a/b = 1 + 2.346(f/f_{min} - 1)^{0.5} + 8.297(f/f_{min} - 1) + 8.4(f/f_{min} - 1)^2 - 0.4589(f/f_{min} - 1)^3 + 0.0314(f/f_{min} - 1)^4 \quad (16)$$

Equations rearranged from Cantor and Schimmel (*63*) yield an estimate of the maximum length (l):

$$l = (8(a/b)^2)^{1/3}M(1 - V_a\rho_a)/(6\pi\eta_a N_o S_{w,20} f/f_{min}) \quad (17)$$

A more refined estimate of the protein's hydrodynamic shape incorporates protein hydration that is calculated from the amino acid composition (accurate to ±10%). This method yielded values of hydration (δ) of 0.438 g of H_2O/g of protein for NA3 and 0.436 g of H_2O/g of protein for NA4. The frictional ratio was calculated by eq 15. The dimensions (a_h/b_h and l_h) for hydrated prolate ellipsoid were calculated based on eqs 16 and 17 and multiplying f/f_{min} by the correction factor for hydration $((V_a + \delta/\rho_a)/V_a)^{1/3}$.

Cosedimentation Binding Assays. Actin (0.95 μM) cosedimented with varying concentrations of nebulin fragments (up to 12 μM) after 1 h at 100000*g* in a Beckman airfuge. After removing the supernatants, a fixed volume of 6 M urea, 10 mM imidazole (pH 7.0), and 0.1 mg/mL bovine serum albumin (BSA) (an internal standard to control for dilution and protein recovery) was added to solubilize the pellets overnight at 4 °C. SDS−PAGE (12%) separated the proteins in both the pellets and supernatants (*44*). Densitometry, by a flat-bed scanner system previously described (*45*), of Coomassie Blue stained gels with standard curves of nebulin fragments, actin, and bovine serum albumin indicated the amounts of proteins in the pellets and supernatants. Less than 10% of the total nebulin fragment pelleted and/or adsorbed to the centrifuge tube walls in the absence of actin or myosin. The concentration of unpelleted actin was determined from the supernatants, and this value was subtracted from the total actin. The binding data were analyzed by a model that assumes one class of independent binding sites for the reaction:

$$B \overset{K_d}{\rightleftharpoons} P + F$$

The equation used for nonlinear curve fitting (by Curve Fit, K. Raner, 1991) is

$$B = \frac{n\mathrm{A} + K_d + N - \sqrt{(nA + K_d + N)^2 - 4nAN}}{2} \quad (18)$$

where B is the molar concentration of bound nebulin fragments, n is the number of independent nebulin binding sites on actin, A is the total molar concentration of actin, N is the total molar concentration nebulin fragment, K_d is the microscopic (site) dissociation constant $= (N - B)(nA - N)/B$, P is the molar concentration of free nebulin binding sites on actin ($P = nA - B$), and F is the molar concentration of free nebulin fragment. We chose the total protein concentration as the dependent variable, since this is more precisely measured than the calculated free concentration and thus more suitable for numerical analysis. Curve-fitting yielded both a dissociation constant and a binding stoichiometry.

ELISA Binding Assays. Microtiter plate assays were performed by first coating plates with 0.1 mL of 1.5 μM NA3 overnight at 4 °C in 1 mM $CaCl_2$ and 10 mM imidazole (pH 7.0) followed by washing three times with TBS (150 mM NaCl, 0.05% Tween-20, 10 mM Tris-HCl, pH 7.4). Copper staining on a duplicate plate (*45*) revealed the amount of adsorbed NA3 (6.5 ± 0.3 ng/well). TBS buffer with 0.2% BSA preblocked the plates for 1 h at 37 °C. Actin (0−12 μM in G-buffer, 0.2 mM $CaCl_2$, 0.5 mM β-mecaptoethanol, 0.2 mM ATP, 2 mM Tris-HCl (pH 7.6), and for F-actin, 2 mM $MgCl_2$) incubated in the wells at 20 °C for 1 h. Mouse monoclonal antibodies JLA20 against actin (*46*) and peroxidase-conjugated secondary antibodies incubated sequentially for 1 h at 37 °C in the TBS blocking buffer with microtiter wells washed three times between each addition. Color development of 2,2′-azinobis(3-ethylbenzthiazoline-6-sulfonic acid) monitored at 405 nm at 4-min intervals with an EIA Reader (BioTek Instruments Inc., Burlington, VT) yielded rates based on linear curve fitting ($r^2 > 0.95$), after subtracting out background rates from wells without coated NA3.

ActoS1 ATPase Assays. ATPase activities of fixed 2.0 μM actin and varied S1 or of fixed 0.5 μM S1 and varied actin concentrations, less the basal magnesium ATPase activity of S1 in the absence of actin, produced actin-activated

ATPase activities. The malachite green assay determined the amount of phosphate released after the addition of ATP (2 mM) at 25 °C to the reaction mixture in 2 mM $MgCl_2$, 1 mM $CaCl_2$, and 10 mM imidazole (pH 7.0).

Actin Polymerization. Fluorescent probes IANBD (Molecular Probes, Eugene, OR) or *N*-(1-pyrene)iodoacetamide (Molecular Probes) labeled cysteine 374 on actin prepolymerized at 2 mg/mL by the addition of 2 mM $MgCl_2$ to G-buffer (0.2 mM $CaCl_2$,0.2 mM ATP, 0.5 mM β-mercaptoethanol, 2 mM Tris-HCl, pH 7.6) for 1 h and then incubated for 16 h at 23 °C with 0.33 mM of either IANBD or *N*-(1-pyrene)iodoacetamide. The F-actin, pelleted at 100000*g* for 1 h at 4 °C, was homogenized in G-buffer and dialyzed against the same buffer for 2 days at 4 °C. A final ultracentrifugation at 100000*g* for 2 h removed minor amounts of aggregated material from the G-actin. The extent of IANBD incorporated, as determined from absorbance at 472 nm with an extinction coefficient of 23 000 M^{-1} cm^{-1}, corresponded to a 1:1 conjugate of 74% of the actin. The fraction of actin modified by pyrene iodoacetamide in different preparations ranged from 40% to 55%, as determined spectrophotometrically using an extinction coefficient of 28 000 M^{-1} cm^{-1} at 344 nm (*32*).

A Zeiss Universal microscope equipped with a DAGE 66 ISIT video camera detected the fluorescence of IANBD-labeled actin. A Scion AG5 frame grabber digitized video images of the actin filaments into public domain NIH Image version 1.54 analysis software. In-house macros, AutoTrack, previously described (*25*), quantified the lengths of fluorescent images.

An SLM 8000 spectrofluorometer (SLM Instruments, Inc., Urbana, IL) measured the fluorescence emission intensity at 410 nm of pyrene-labeled actin in 1-mL quartz cuvettes at 25 °C excited by 365 nm light. The spectrofluorometer produced time-based fluorescence profiles with 1 s integration times demonstrating an increase of pyrene fluorescence with actin polymerization.

RESULTS

Experimental Design. Three types of fluorescence measurements that have been used extensively in actin−myosin interactions were applied to analyze the interactions between actin and the myosin head under the influence of nebulin fragments. First, the quenching of the fluorescence intensity of pyrene iodoacetamide attached to cysteine 374 of actin reports quantitatively the fraction of actin bound by the strong-binding S1 (*47*, *48*). Second, the increase in the fluorescence polarization of IAEDANS-labeled S1 upon binding F-actin indicates a slowing of the rotation of the probe in the resulting actoS1 complexes (*34*). Third, the fluorescence resonance energy transfer between IAEDANS conjugated to cysteine 707 (SH1) of S1 and IANBD conjugated to cysteine 374 of actin was used to measure the separations between these residues. Additional experimental evidence is presented to characterize the stoichiometry of the associations of the nebulin fragments with actin that influence actoS1 interactions.

Nebulin Fragments Cause Little Change in Equilibrium Binding of S1 to Actin. The quenching of the fluorescence intensity by the strong binding of S1 to pyrene-actin labeled on cysteine 374 is illustrated in Figure 1A. The maximum

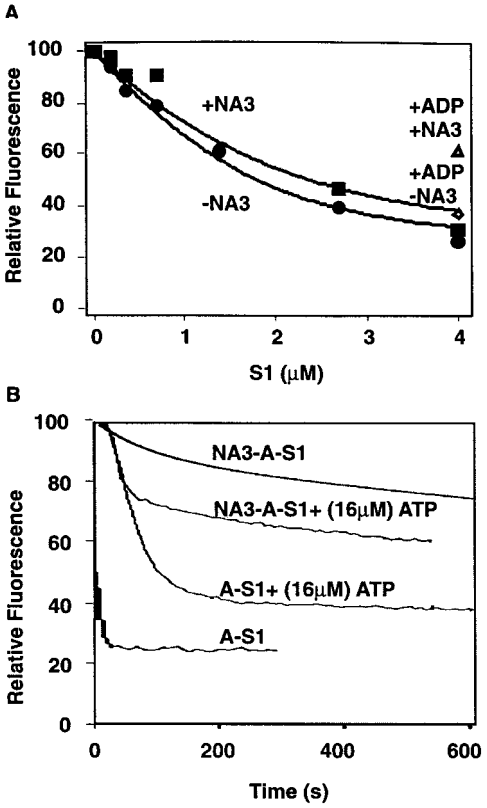

FIGURE 1: Effects of NA3 on the equilibrium binding and rate of association of pyrene−actin and S1 upon adding ATP. (A) Binding of NA3 to actomyosin complexes. S1 (0−4.0 μM) is incubated with a fixed concentration of pyrene−actin (1.7 μM) with or without 1.8 μM NA3. The assay buffer contains 1 mM $CaCl_2$, 2 mM $MgCl_2$, and 10 mM imidazole, pH 7.0. Fluorescence intensity at 407 nm is recorded after a stable plateau intensity is reached and is normalized to the value of pyrene−actin fluorescence in the presence or absence of NA3. The curve fitting by a simple binding isotherm is described in the text. Binding of NA3 has minimal effect on the extent of quenching of pyrene−actin by S1. (B) Effect of NA3 on the rate of association of actin and myosin. The assay buffer contains 1 mM $CaCl_2$, 2 mM $MgCl_2$, and 10 mM imidazole, pH 7.0. NA3−A−S1: Pyrene actin (1.7 μM) is premixed with NA3 (1.8 μM) and incubated 5 min. S1 (4.0 μM) is then added to start the quenching at time zero on the plot. A−S1−NA3 + 16 μM ATP: Pyrene actin and S1 are premixed and added to NA3, and 16 μM ATP is added to dissociate actin and S1. Time zero indicates reassociation begins after the ATP is hydrolyzed. A−S1 + 16 μM ATP: Pyrene actin and S1 are mixed, and 16 μM ATP is added to dissociate actin and S1. Time zero indicates reassociation begins after the ATP is hydrolyzed. A−S1: Pyrene actin is mixed with S1 to start the quenching at time zero on the plot. Quenching is too rapid to resolve on this time scale. The rate of fluorescence quenching of pyrene actin complexes by S1 is greatly slowed by NA3 especially in the absence of added ATP.

quenching of pyrene actin fluorescence by S1 at high ratios of S1 to actin is approximately 80%, in good agreement with that reported by Kouyama and Mihashi (*47*). The data in Figure 1A are fit by a simple binding isotherm (see Materials and Methods). From nonlinear curve fitting, the estimated dissociation constant of actin and S1 is 0.4 ± 0.1 μM (r^2 = 0.987), in reasonable agreement with measurements in the literature performed in the presence of low concentrations of ADP (*48*−*50*). Upon the addition of NA3 (1.8 μM), the quenching of pyrene actin (1.7 μM actin) by S1 (4.0 μM S1) is affected slightly, dropping from 74% to 70%. The same experiment using a 7-module fragment, NA4 (*7*, *25*), produces similar results in that the fluorescence quenching

curves from titrating with S1 in the presence or absence of NA4 are not significantly different (data not shown).

In a control experiment, the presence of NA3 (1.8 μM) is found to increase the fluorescence intensity of the pyrene actin (1.7 μM) by only 13% ± 1% (data not shown). Since the critical concentration of the magnesium-polymerized actin in the same buffer is little affected by NA3 in cosedimentation assays (*25*), this increase might reflect a change in the probe environment upon NA3 binding. Given the much smaller change in fluorescence induced by NA3, as compared to the 80% quenching of pyrene actin by S1, the binding of S1 to actin in the presence of NA3 may also be estimated by the quenching of pyrene actin fluorescence by S1. We normalize the fluorescence to the value of actin with NA3 in the absence of S1 and use the percent quenching as a measure of the strong binding of S1 to actin in the presence of NA3. Under such conditions, the addition of NA3 increases only slightly the dissociation constant to 0.8 ± 0.2 μM ($r^2 = 0.955$). A reduction in the affinity of S1 for actin by the addition of ADP increases the effect of NA3 on actoS1 binding (Figure 1A).

NA3 Slows the On-Rate of Strong S1 Binding to Actin. The quenching of pyrene actin by S1 in the absence of NA3 is nearly instantaneous and can be time-resolved only with the use of stop-flow equipment (*48*). In contrast, when NA3 (1.8 μM) is premixed with actin (1.7 μM) prior to the addition of S1 (4.0 μM), the fluorescence intensity is quenched gradually over a course of several hours depending on the S1 concentration. Eventually, the relative fluorescence falls to the same level as the sample prepared by adding NA3 to the actoS1 complex. Early time points of the course of this quenching can be well fit by the sum of two exponential decays (Materials and Methods). The larger rate constant k_1 has roughly similar values at both S1 concentrations tested: $1.1 \times 10^{-2} \pm 0.1 \times 10^{-2}$ s^{-1} ($a = 0.27 \pm 0.01$) and $0.6 \times 10^{-2} \pm 0.3 \times 10^{-2}$ s^{-1} ($a = 0.11 \pm 0.02$) for S1 concentrations of 4.0 and 1.4 μM, respectively. The smaller rate constant k_2 varies from $2.1 \times 10^{-4} \pm 0.2 \times 10^{-4}$ s^{-1} ($b = 2.14 \pm 0.01$) at 4.0 μM S1 to $0.86 \times 10^{-4} \pm 0.15 \times 10^{-4}$s^{-1} ($b = 2.39 \pm 0.02$) at 1.4 μM S1. The dependence of k_2 on S1 concentrations is roughly linear, suggesting that k_2 may be related to the on-rate of S1 binding to actin in the presence of NA3. If this is the case, then the observed on-rate constant for S1 binding to actin in the presence of NA3 would be k_2 divided by the S1 concentration which is 57 ± 4 M^{-1} s^{-1}. Clearly, premixing actin with NA3 significantly reduces the on-rate of S1 to actin, which in the absence of NA3 is nearly diffusion-limited (10^7−10^8 M^{-1} s^{-1}) (*50*). The significance of k_1 is obscure, and we speculate that it may be related to the observed off-rate constant for NA3 detachment from either actin or S1. The very slow on-rate of S1 binding to actin premixed with NA3 also permits comparative measurements of both polarization and fluorescence energy transfer before (S1−ANA3) and after (S1−A−NA3 and S1−NA3−A) equilibrium is reached. These data are in agreement with the kinetic measurements and are illustrated in Figure 2B,C.

ATP Dissociates S1 Binding to Actin in the Presence of NA3. As expected, when ATP is added to actoS1, the S1 dissociates rapidly from pyrene actin, and the fluorescence intensity returns to within 96 ± 7% of that of pyrene actin alone. When ATP is added to the NA3−actoS1 complex, the fluorescence intensity also returns rapidly to 97 ± 3% of that of the NA3−actin complex (Figure 1A). Indeed, the fluorescence intensity in the presence of ATP is the same, whether NA3 is premixed with actin before adding S1. These data indicate that NA3 does not impede the dissociation of the actoS1 complex by ATP, which weakens the binding of S1 to actin by 2−3 orders of magnitude.

The effect of ATP on the interaction of S1 to actin can be examined in more detail by repeatedly adding increasing amounts of ATP to actoS1 in the presence or absence of NA3. The time course of fluorescence quenching for this type of cycling generally consists of four phases (Figure 1B).

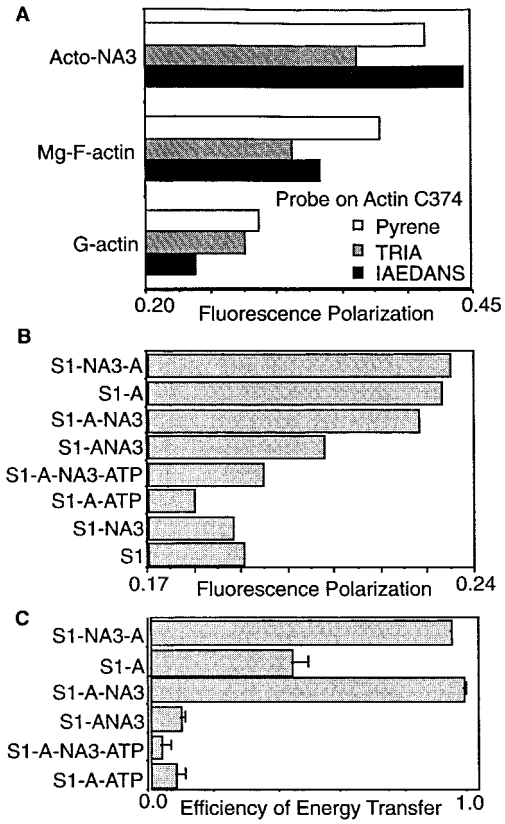

FIGURE 2: Effects of NA3 on actin and its interaction with S1 as revealed by fluorescence polarization and fluorescence resonance energy transfer. (A) Effects of NA3 on the polarization of C374-labeled actin. The polarizations of actins labeled on C374 with pyrene, TRIA, or IAEDANS are measured in G-buffer (G-actin), G-buffer with 2 mM $MgCl_2$ (Mg-F-actin), or G-buffer and equal molar NA3 with 2 mM $MgCl_2$ (Acto-NA3). Estimated errors in polarization are less than 0.01. (B) Effects of NA3 on actoS1 binding as monitored by fluorescence polarization. Fluorescence polarization for IAEDANS-labeled S1 (1 μM in 1 mM $CaCl_2$, 2 mM $MgCl_2$, and 10 mM imidazole (pH 7.0) is measured at 483 nm (excited at 370 nm). F-actin (1.0 μM; abbreviated as A), NA3 (2.0 μM), ATP (2.5 mM), and/or premixed F-actin with NA3 (abbreviated as ANA3) are added in the order as specified by dashes. The standard deviation for separate measurements does not exceed ±0.007 polarization units in all cases. (C) Effects of NA3 on the efficiencies of fluorescence energy transfer between IAEDANS-S1 and IANBD-F-actin. Quenching of the fluorescence of IAEDANS on SH1 of S1 with IANBD on actin C374 is measured in 1 mM $CaCl_2$, 2 mM $MgCl_2$, and 10 mM imidazole (pH 7.0). F-actin (1.0 μM; abbreviated as A), NA3 (2.0 μM), ATP (2.5 mM), and/or premixed F-actin with NA3 (abbreviated as ANA3) are added to S1 (0.5 μM) in the order specified by dashes. Error bars represent the range of difference between means from efficiencies determined at two excitation wavelengths (336 vs 370 nm).

When 16 μM ATP is added to actoS1, a rapid rise in fluorescence ensues (phase I), reflecting the dissociation of S1 from actin. A slight intensity decrease follows (phase II), probably resulting from the increasing ratios of ADP to ATP as ATP is being hydrolyzed, since S1 (ADP) binds actin stronger than S1 (ATP) (*49*). This phase is followed by a rapid drop in fluorescence (phase III, Figure 1B), as ATP hydrolysis approaches completion and the strong binding of S1 to actin occurs. The fluorescence eventually reaches a new plateau (phase IV, Figure 1B), reflecting the attainment of complete strong binding. Time courses of fluorescence quenching, when ATP is added to actin−S1−NA3 complexes, display qualitatively similar changes, with noticeable difference in the duration and rate of changes for phases II, III and IV. In the presence of NA3, phase II lasts three to four times longer (data not shown) and has a slower rate of fluorescence quenching (0.013% s^{-1} vs 0.024% s^{-1}, presence vs absence, respectively). These results are consistent with our observation that NA3 causes a 3-fold decrease in total ATPase activity under similar conditions (*25*). The drop in fluorescence intensity during phase III is much smaller at the onset of phase IV. Accordingly, the plateau intensity of phase IV is higher. The higher fluorescence of phase IV likely reflects the decrease in affinity of S1 (ADP) for actin that is significantly enhanced by NA3 (cf. Figure 1A).

The reassociation of S1 and NA3−actin is more rapid when S1 hydrolyzes a small concentration of ATP in contrast to the case where S1 binds to NA3−actin in the absence of ATP (data not shown). Although NA3 clearly affects the polarization of fluorescent probes on C374 of actin (Figure 2A), these perturbations of actin structure do not prevent the reassociation of S1 with actin following hydrolysis of small amounts of ATP. The initial rates of pyrene actin fluorescence quenching are nearly identical in the presence and absence of NA3 when ATP is present, and both of these rates are strikingly more rapid than when S1 is added to NA3−actin in the absence of ATP (Figure 1B). These results suggest that NA3 may affect the way that S1 binds to actin and perhaps helps to prevent specifically the binding of S1 lacking bound ADP−Pi.

NA3 Does Not Dissociate S1 from Actin. The polarization of fluorescently labeled S1 is used to detect binding of S1 to actin. Since the large actoS1 complex rotates slower than S1 alone, the rotation of a fluorescent probe attached to S1 is reduced in this complex, resulting in an increase in polarization. Indeed, fluorescence polarization of S1 (1 μM, labeled with IAEDANS) strongly bound to F-actin (1 μM) is 0.233 at 483 nm as compared with 0.191 ± 0.007 for S1 alone (Figure 2B).

NA3 does not change the polarization of S1 in the absence of actin (S1−NA3 = 0.188) (Figure 2B). When NA3 is added to actoS1, polarization (S1−A−NA3 = 0.228) also does not change appreciably. The same results are obtained when NA3 is premixed with S1 prior to adding actin (S1−NA3−A = 0.235). Yet, when actin is premixed with NA3 and then added to S1 (S1−A−NA3), the polarization measured immediately thereafter is only 0.208 as compared with 0.232 when NA3 is not premixed with actin. Very similar effects of NA3 are observed by FRET measurements between actin and S1 that confirm these effects of the order of mixing on the association of S1 with actin in the presence of NA3 (Figure 2C). Thus, premixing actin and NA3 interferes with the binding of S1 to F-actin by a mechanism that could involve a direct alteration of the actoS1 complex or a bundling of actin that reduces the accessibility of interactions. The normal rates of dissociation and reassociation of S1 to actin upon the addition of small amounts ATP provides evidence that steric hindrance is probably not the reason for the slow on-rate of S1 binding to actin in the absence of ATP, while FRET results suggest that the structure of the actoS1 complex is altered in the presence of nebulin fragments (Figure 2C).

In the presence of ATP, the order of mixing NA3, actin, and S1 does not affect polarization. When ATP is added, S1 dissociates from F-actin and fluorescence polarization drops to 0.180, comparable to the 0.191 ± 0.007 value for S1 without ATP or actin. The smaller polarization of S1 (ATP) may reflect the increased mobility of the probe site (SH1) in the presence of ATP (*34*, *51*, *52*). The polarization of S1 with actin and ATP increases from 0.180 (S1−A−ATP) to 0.194 ± 0.004 in the presence of NA3 (S1−A−NA3−ATP). This increase in polarization supports the assertion that NA3 links S1 to actin in the presence of ATP, which is consistent with previous results from binding studies (*25*).

NA3 Shortens the Distance between SH1 of S1 and C374 of Actin in the Strongly Bound Complex. The structure of actoS1 complexes in the presence of NA3 is further characterized by estimating the distance between cysteine 374 on actin and cysteine 707 (SH1) on S1 by fluorescence resonance energy transfer. The emission spectrum of IAEDANS strongly overlaps with the absorption spectrum of IANBD (Figure 3A) and is thus optimal for transfer efficiency. Since overlap between the emission spectra of IAEDANS and IANBD makes it difficult to accurately estimate E from increases in acceptor emission, E is measured by the decrease in fluorescence of the donor in the presence of acceptor. The titration of donor (IAEDANS) labeled S1 (0.5 μM) with strongly bound acceptor (IANBD) labeled F-actin yields a plateau in the quenching of fluorescence emission of the donor between 0.5 and 1 μM F-actin (data not shown). A concentration of 1.0 μM F-actin therefore saturates the S1 binding sites and quenched fluorescence emission of the donor by 33 ± 4%. By assuming that the IANBD-labeled actin and unlabeled actin bind IAEDANS-labeled S1 with similar affinities under strong binding conditions (*49*, *53*) and that energy transfer occurs only between the one acceptor and donor pair that are closest in proximity, the corresponding efficiency of transfer is 33%/74% = 0.44 per donor/acceptor pair, since 74% of the actin is labeled by IANBD. This value concurs with an efficiency of 0.43 ± 0.05 obtained from steady-state measurements of energy transfer between IAEDANS-labeled F-actin and IANBD-labeled S1 by Miki and Wahl (*54*). The addition of NA3 (2.0 μM), either to actoS1 complex or to S1 prior to actin addition, causes a dramatic increase in the transfer efficiency (S1−A−NA3 or S1−NA3−A in Figure 2C) to greater than 0.9. Yet, when actin is premixed with NA3 and then added to S1 (S1−A−NA3) and the energy transfer is measured immediately thereafter, the apparent efficiency of transfer is only about 0.1. Similar values are obtained upon the addition of ATP (2 mM) to dissociate strong binding actoS1 complexes that reduce the transfer efficiency to less than 0.1 (S1−A−ATP and S1−A−NA3−ATP in Figure

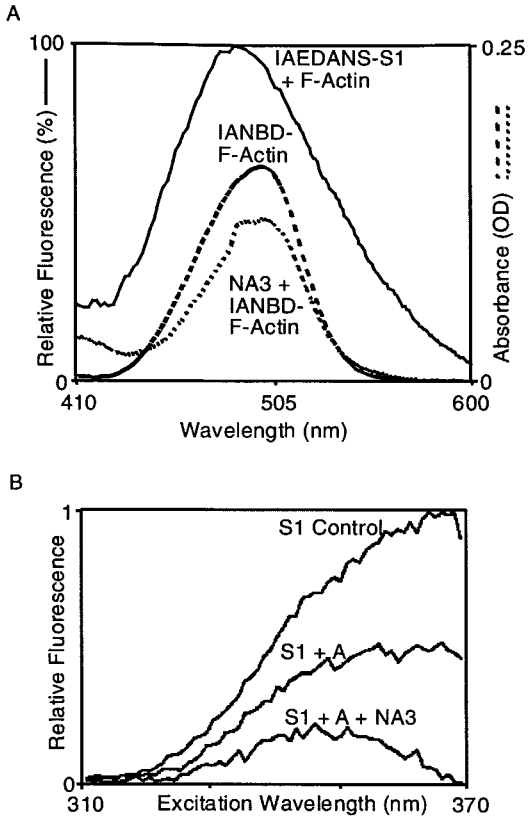

FIGURE 3: Effect of NA3 on fluorescence energy transfer between S1 and actin. (A) Fluorescence spectrum of IAEDANS−S1 (donor), absorption spectra IANBD−F-actin (acceptor), and excitation spectra used in energy transfer studies. The overlap of IAEDANS emission and IANBD absorption is substantial. The corrected fluorescence emission spectrum of labeled S1 is not affected significantly by either unlabeled F-actin or NA3 (not shown for clarity). NA3 affects slightly the normalized (OD in mL/mg) absorbance spectrum of F-actin when compared with that of F-actin in the absence of NA3. All spectra are measured in 1 mM $CaCl_2$, 2 mM $MgCl_2$, and 10 mM imidazole (pH 7.0). (B) Excitation wavelength dependence of the efficiencies of fluorescence energy transfer between IAEDANS-S1 and IANBD-F-actin. Quenching of IAEDANS fluorescence at 472 nm by donor IANBD on C374 of actin is represented by excitation difference spectra between the presence and absence of IAEDANS attached to C 697 on myosin subfragment 1 (S1). When NA3 is added, the degree of energy transfer is greatest, but the amount of donor quenching relative to the control varies substantially with excitation wavelength. The proposed interpretation is that varying excitation wavelengths excite donor dipoles with different orientations that can influence energy transfer (see eq 1).

2C). It is worth noting that, in the presence of ATP, S1 is mostly dissociated from actin, thus the efficiency of energy transfer for the transiently bound actoS1 complex is higher than the apparent values presented in Figure 2C. The apparent value corresponds to an ensemble average of bound and unbound states.

Extensive energy transfer studies have been done to measure the distance directly between SH1 (S1) and cysteine 374 (actin) in actoS1 complex with different sets of donor-acceptor pairs on these sites (*39*, *55*). These values average 50 ± 5 Å by assuming $\kappa^2 = {}^2/_3$. Indirect estimation by distance geometry from other donor-acceptor sites on actin and S1 yields similar separation distances of 50 (*39*) and 52 Å (*55*) when $\kappa^2 = {}^2/_3$. The calculated spectroscopic distances are also in good agreement with the structural model of the actoS1 complex (*56*−*61*). The FRET values in Table 1 in the absence of NA3 are in excellent agreement with the literature values.

The addition of NA3 to actoS1 and the addition of actin to premixed NA3−S1 yield very similar $R_{2/3}$ values (19.9 ± 2.6 and 25.3 ± 0.2 Å, respectively) that are strikingly lower than the 45.2 Å spacing for actoS1. Even in the unlikely event that $\kappa^2 = 4$, its theoretical maximum, the distance between fluorophores attached to SH1 and C374 must be less than 27 Å in the presence of NA3 (Table 1), which is significantly less than the 50 Å distance in the strong binding complex in the absence of NA3. When NA3 is premixed with actin prior to S1 addition, $R_{2/3}$ increases to 59.6 ± 1.5 Å. Even higher values are obtained when ATP is added to actoS1 ($R_{2/3} = 66.4 \pm 4.5$ Å) or to actoS1 plus NA3 ($R_{2/3} = 71.5 \pm 8.2$ Å). These values represent ensemble average of unbound and bound S1 on actin in the presence of ATP. Unfortunately, these ensemble average distances are too long (relative to R_o) to be useful to determine the distance between the donor-acceptor pair in the presence of NA3 and ATP. Further complications in quantitative interpretations of the data arise from the apparent structural changes in actin upon nebulin fragment binding as detected by fluorescence polarization measurements (Figure 2A).

Additionally, we apply the technique of varying the excitation wavelengths of the donor fluorophore, IAEDANS, to preferentially excite dipoles with a different set of orientations (as judged by an observed difference in fluorescence polarization) (*42*) to examine the effect of dipole orientation on *R* values (Figure 3B; *62*). We observe a change in the calculated $R_{2/3}$ distance between excitation at 336 nm versus excitation at 370 nm (Table 1) particularly when NA3 is present. This change is illustrated most strikingly in Figure 3B by comparing excitation difference scans of IANBD-actin with IAEDANS-S1 (and subtracting a background excitation scan of the same but with unlabeled S1 substituted for IAEDANS-S1) in the presence and absence of NA3. Nebulin fragment NA4 also increased the efficiency of energy transfer between probes on cysteine 697 on S1 and cysteine 374 on actin, so that the efficiencies of transfer were 0.64 and 0.48 when excited at 370 and 336 nm, respectively, which compare to control values in the absence of NA4 of 0.49 and 0.48 at the same wavelengths. Thus, the results using NA3 and NA4 are qualitatively similar in that the efficiency of transfer is increased in the presence versus the absence of nebulin fragment. The quantitative variability with different excitation wavelengths suggests that nebulin fragments affect the orientation between the fluorescent probes on S1 and actin, and it is possible that the nebulin fragments either affect the orientation factor or the distance between donor and acceptor fluorophores differently.

Nebulin Fragments Are Elongated Monomers. High-speed equilibrium centrifugation of NA3 and NA4 reveals that these nebulin fragments are primarily, if not exclusively, monomeric. Their calculated molecular masses are 31 285 and 27 779 Da, respectively, based on their amino acid compositions, which agree well with their observed molecular masses of 37 000 ± 6000 Da for NA3 and 35 000 ± 5000 Da for NA4 from equilibrium centrifugation (see Figure 4A). This agreement indicates that the nebulin fragments have little or no self-association. Since equilibrium centrifugation yields weight-averaged molecular weights, the maximum fraction of multimeric complexes are 10 ± 10% for NA3 and 15

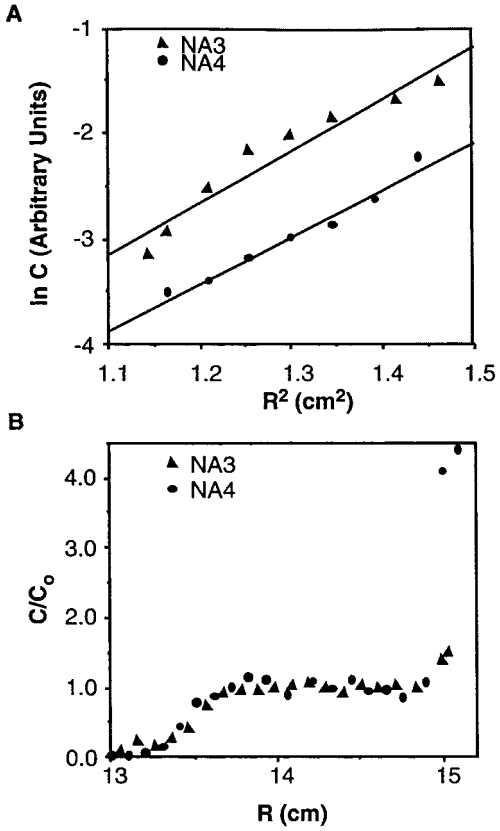

FIGURE 4: Sedimentation studies of size and shape. (A) Equilibrium sedimentation of NA3 and NA4. Protein distribution profiles are obtained with a Beckman Airfuge at 54000 rpm for 80 h at 300 K in 20% sucrose, 2 mM $MgCl_2$, 1 mM $CaCl_2$, and 10 mM imidazole (pH 7.0). The slopes of data as determined by linear regression are 4.9 ± 0.6 cm^{-2} (r^2 = 0.920) and 4.7 ± 0.5 cm^{-2} (r^2 = 0.973) for NA3 and NA4, respectively. See text for calculations of molecular weights. (B) Velocity sedimentation of NA3 and NA4. Protein distribution profiles are obtained with a Beckman SW41 swinging bucket rotor at 35 000 rpm for 18 h at 20 °C in 20% sucrose, 2 mM $MgCl_2$, 1 mM $CaCl_2$, and 10 mM imidazole (pH 7.0). The trailing boundary is 0.48 ± 0.05 cm from the meniscus for both NA3 and NA4 by interpolation of data points. See the text for calculation of the sedimentation coefficients.

± 11% for NA4. Further evidence supporting the homogeneous nature of the nebulin fragment's molecular weight is that the plots show no sign of an upward curvature. If higher molecular weight species were also present, they would preferentially sediment, which would be manifested as a concave curve. Since the estimated fraction of multimeric species is very low and could easily be due to experimental error, subsequent calculations assume that the monomeric molecular weights are correct.

Sedimentation velocity measurements and calculated hydrodynamic parameters indicate that the nebulin fragments are highly elongated (Table 2). The water-corrected sedimentation coefficients for NA3 and NA4 are both 1.1 ± 0.1 S based on displacement of the trailing boundary after 18 h (see Figure 4). In particular, frictional coefficient ratios are 3.27 for NA3 and 2.96 for NA4, which are significantly greater than that for a highly asymmetric protein, tropomyosin (2.65). The incorporation of protein hydration in the calculation lowers slightly this ratio to 2.79 for NA3 and 2.53 for NA4, indicating again that these fragments are highly elongated in aqueous solution even in the absence of actin.

Table 2: Hydrodynamic Properties of Nebulin Fragments

fragment	NA3	NA4
amino acids (aa)	269	242
M_r equil sed (calcd)	37 kDa (31 kDa)	35 kDa (28 kDa)
$S_{w,20}D_{w,20}$	1.1 S	1.1 S
anhydrous rod	3.2×10^{-7} cm^2/s	3.6×10^{-7} cm^2/s
prolate axial ratio (a/b)[a]	62.1	49.8
max length (l)[a]	65.4 nm	54.3 nm
l/aa[a]	0.243 nm/aa	0.224 nm/aa
hydrated rod		
prolate axial ratio (a_h/b_h)[a]	43.6	34.7
max length (l_h)[a]	60.5 nm	50.0 nm
l_h/aa[a]	0.225 nm/aa	0.207 nm/aa

[a] Assuming a rigid rod model.

On the basis of the calculated dimensions of the superrepeat (Table 1), the 22 superrepeats of human nebulin that comprise about 80% of the total sequence may extend as far as 1.1 μm, which is almost the thin filament length in skeletal muscle.

Nebulin and Actin Interaction. Cosedimentation assays of NA4 with actin in 2 mM $MgCl_2$, 1 mM $CaCl_2$, and 10 mM imidazole (pH 7.0) yield a dissociation constant of 0.6 ± 0.1 μM and stoichiometry of 1.47 ± 0.09 actins per NA4 (see Figure 5A). These values compare to a dissociation constant of 1.1 ± 0.1 μM and a stoichiometry of one actin per NA3 determined previously by cosedimentation assays under the same buffer conditions. An identical dissociation constant of 1.2 ± 0.2 μM is derived from the isotherm of actin binding to NA3 in ELISA as shown in Figure 5B.

ELISA allows a comparison of the binding of monomeric actin and F-actin to solid-phase NA3. When a protomer of F-actin binds to solid-phase NA3, the entire F-actin filament is captured in the well; however, during washing and incubations of the microtiter plate with antibodies, the bound F-actin is diluted below its critical concentration and depolymerizes, leaving only the bound actin monomer in the well. The greater the amount of initially bound actin protomers in either the G or F-actin buffer conditions, the greater the amount of actin is left bound after the subsequent washings. Thus, ELISA response is proportional to the bound actin monomer whether the actin is initially monomeric or filamentous. Therefore, it is not surprising that NA3 binds monomeric actin and F-actin equally well yielding similar ELISA readings as illustrated in Figure 5B.

The polymerizing effect of NA3 on G-actin is evident from fluorescence microscopy of IANBD-labeled actin (see Figure 6). As a control, the polymerization of G-actin (2 μM) by the addition of 2 mM $MgCl_2$ requires 1−2 h to form filaments of 2.2 ± 0.1 μm in length. By contrast, the addition of NA3 or NA4 to actin (2 μM) in G-buffer induces rapid formation of polymers of 3.8 ± 0.4 μm and 4.3 ± 0.5 μm in length, respectively, within 2 min. This rapid polymerizing ability of NA3 and also NA4 is confirmed by measuring the enhancement of pyrene fluorescence from labeled actin which indicates actin polymerization (see Figure 7A). The time required for 50% enhancement of pyrene actin fluorescence is 1100 s for magnesium-induced polymerization but only 30 s for polymerization by NA3 or NA4 (Figure 7A). The addition of nebulin fragments to pyrene F-actin causes less than a 15% increase in fluorescence intensity in comparison to an observed 2000% increase in pyrene fluorescence during

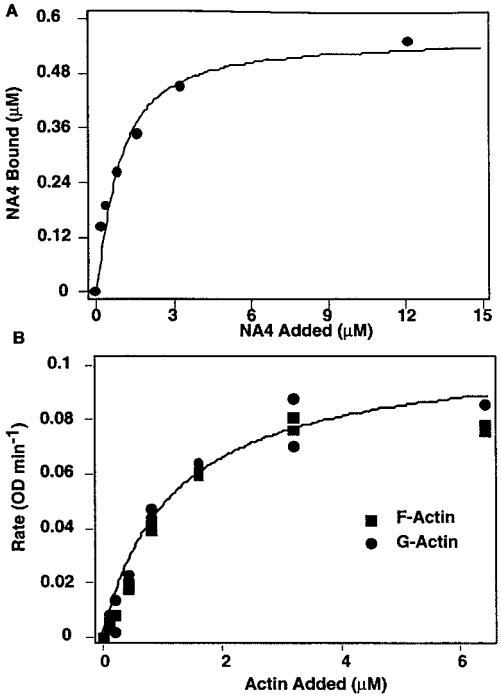

FIGURE 5: Binding of a nebulin superrepeat, NA4, to F-actin. (A) Cosedimentation binding isotherm. NA4 (0−12 μM) is incubated for 15 min with 0.95 μM actin cosedimented with F-actin in a Beckman airfuge at 100000*g* for 1 h at 300 K in 20% sucrose, 2 mM $MgCl_2$, 1 mM $CaCl_2$, and 10 mM imidazole (pH 7.0). Pellets are analyzed by SDS−PAGE, Coomassie blue staining, and densitometry. The binding isotherm fit by nonlinear regression indicates a dissociation constant of 0.6 ± 0.1 μM ($r^2 = 0.976$), indicating a high-affinity interaction. (B) ELISA binding isotherm. NA3 preadsorbed to a microtiter plate bound actin (0−6.4 μM) in G-buffer or F-actin in G-buffer (0.2 mM $CaCl_2$, 2 mM ATP, 0.5 mM β-mercaptoethanol, 2 mM Tris-HCl, pH 7.6) plus 2 mM $MgCl_2$ during a 45-min incubation at room temperature. Bound actin detected by monoclonal antibodies and ELISA yields binding isotherms with dissociation constants of 1.2 ± 0.2 μM ($r^2 = 0.973$) fit by nonlinear regression. NA3 binds both monomeric and F-actin with high affinity.

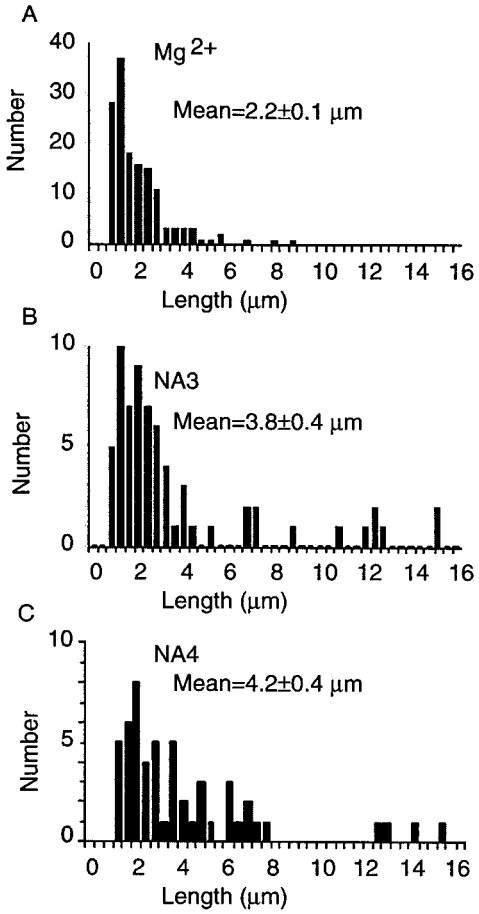

FIGURE 6: Effect of NA3 on the length distribution of F-actin. IANBD-labeled actin (2 μM) in G-buffer (0.2 mM $CaCl_2$, 2 mM ATP, 0.5 mM β-mercaptoethanol, 2 mM Tris Cl, pH 7.6) polymerizes at 20 °C upon the addition of (A) 2 mM $MgCl_2$ for 2 h; (B) 2 μM NA3 for 2 min; or (C) 2 μM NA4 for 2 min. A distribution histogram and the mean value of measured actin filament lengths by fluorescence microscopy are illustrated for each case.

actin polymerization; therefore, NA3 and NA4 do not significantly affect the rate of increase in fluorescence beyond inducing polymerization. Similarly, the difference in fluorescence intensity of NA3 or NA4 polymerized pyrene actin over that of that of magnesium-polymerized pyrene actin is less than 15% (Figure 7A).

There is a nearly linear correlation between the calculated fraction of actin bound by NA3 or NA4 and the increase in pyrene fluorescence (Figure 7). Using binding constants from cosedimentation assays, the calculated fraction of actin bound at different concentrations of nebulin fragment can be plotted against the increase in fluorescence intensity of pyrene actin (Figure 7A,B). This plot indicates that when actin is completely polymerized, only about one NA3 or NA4 is bound per three to four actin protomers (Figure 7C). This functional stoichiometry of three to four actin molecules polymerized per superrepeat is significantly greater than the nearly one to two high-affinity actin binding sites per nebulin superrepeat determined from cosedimentation assays (*25*; Figure 5A). The nebulin superrepeat therefore influences multiple actin monomers during actin polymerization.

Additional support for the idea that the nebulin superrepeat affects the function of multiple actin molecules comes from the kinetic analysis of nebulin inhibition of actin-activated S1 ATPase activity. Nebulin fragments show strikingly different effects in two types of actin-activated ATPase assays. In one type of assay, the S1 concentration is kept constant at a low level while actin concentrations are varied to high levels where a maximum turnover rate is achieved. At the maximum turnover rate, the addition of small amounts of nebulin fragments has little effect on actin-activated ATPase activity (Figure 8A,B). In an inverse type of assay, varying S1 to high levels over a fixed actin concentration produces a condition where actin activation of S1 ATPase activity is highly sensitive to the presence of small amounts of NA3 or NA4 (Figure 8C,D). This effect suggests that the binding of nebulin fragment to actin is critical for its ability to inhibit actin-activated ATPase activity. Indeed, one observes a strong approximately linear correlation between the ratio of NA3 or NA4 to actin and the relative ATPase, defined as the ratio of actin-activated ATPase activity in the presence to that in the absence of nebulin fragment (Figure 8E,F). By comparison, the ratio of NA3 or NA4 to S1 shows virtually no correlation with the relative actin-activated ATPase (Figure 8E,F), even though S1 binds strongly to nebulin fragments.

Analysis of the ATPase data in an analogous fashion to the polymerization data yields similar results (Figure 9). Our

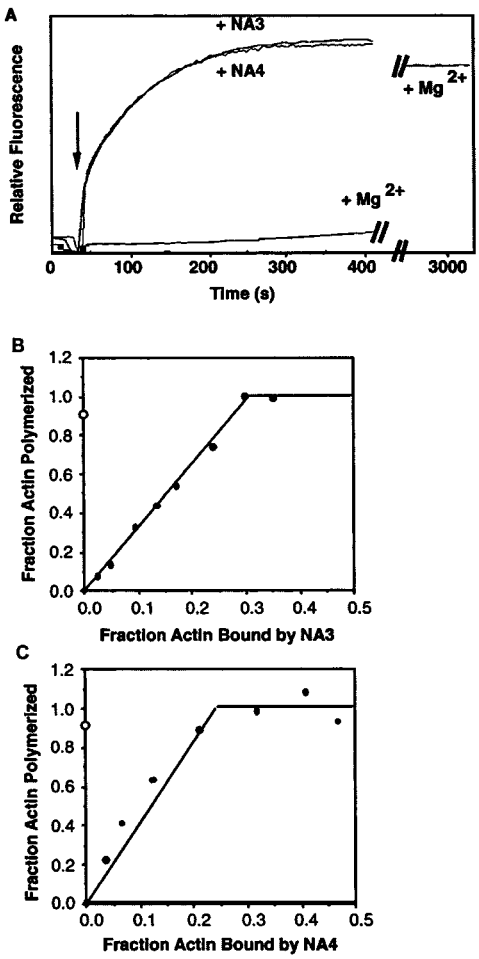

FIGURE 7: Polymerization of pyrene actin by nebulin fragments. (A) Rate of polymerization by fluorescence enhancement. Pyrene actin (2 μM) is diluted into 1 mM $CaCl_2$ and 10 mM imidazole (pH 7.0) (identical results are also obtained in G-buffer, data not shown) polymerized at 25 °C upon the addition of 2 mM $MgCl_2$, 2 μM NA3, or 2 μM NA4 as evidenced by the time-dependent increase in pyrene fluorescence. Arrows indicate the time of addition of the polymerizing reagent during which brief time the fluorescence intensity is not measured. (B, C) Dose-dependent polymerization of actin by NA3 and NA4. Pyrene actin (2 μM) is diluted into 1 mM $CaCl_2$ and 10 mM imidazole (pH 7.0) (identical results are also obtained in G-buffer, data not shown) at 25 °C and polymerizes upon the addition of NA3 (B) and NA4 (C). The fraction of actin polymerized is estimated by normalization to the fluorescence intensity at plateau (indicated by the horizontal bar). The fraction of actin bound by nebulin fragments is calculated from cosedimentation data using the equations described in the text.

previous observation that varying concentrations of S1 does not interfere with the binding of nebulin fragment to actin allows the calculation of the fraction of actin bound by NA3 or NA4 from binding constants as used in Figure 5B. The plots (Figure 9A,B) demonstrate that the fraction of actin bound by nebulin fragment is less than one-half when the relative ATPase is completely inhibited. This result supports the idea that the nebulin superrepeat inhibits multiple actin molecules from activating S1 ATPase activity.

DISCUSSION

The application of various fluorescence techniques yields complementary results that provide further insights into the effects of nebulin fragments on actomyosin interactions. Taken together our data indicate nebulin fragments alter substantially the actoS1 complex: (i) Under strong binding conditions, premixing actin with NA3 prior to adding S1 inhibits the on-rate of strong binding of S1 to actin (fluorescence polarization and pyrene actin data). (ii) When NA3 is added to actoS1 or premixed NA3 and S1 are added to actin, S1 is capable of sustaining a strong bond with F-actin (fluorescence polarization, pyrene actin, and FRET data). (iii) The rate of reassociation between S1 and actin in the presence of NA3 is much faster following the hydrolysis of ATP than under strong binding conditions (pyrene actin data). (iv) Calculated energy transfer distances between S1 and actin are smaller, suggesting that S1 and actin are closer together in the presence versus the absence of NA3. Preliminary data with another nebulin fragment, NA4, yield qualitatively, and in several cases quantitatively, similar results to those obtained with NA3, which supports the view that these effects are a general phenomenon of the nebulin superrepeat. These data are discussed below and summarized schematically in Figure 10.

Nebulin's Interactions with Actin. Two bacterially expressed fragments of human fetal nebulin, corresponding to about one superrepeat each, exhibited nearly identical properties in biochemical and structural assays. Sedimentation experiments indicated that these fragments are monomeric and highly elongated to an extent that is consistent with a single intact nebulin being capable of spanning the entire length of a thin filament. The nebulin fragments induce very rapid polymerization of actin even in G-buffer. Calculations based on cosedimentation binding assays and polymerization of pyrene actin indicate that one nebulin superrepeat supports the polymerization of approximately three to four actin monomers. In addition, the fragments inhibit potently actin's ability to activate S1 ATPase activity. One superrepeat appears to prevent two to three actin molecules from activating S1 ATPase activity. Thus, an elongated nebulin superrepeat appears to influence several actin molecules along an actin filament. These fragments appear to be a good model for understanding the functions of nebulin, which contains 22 superrepeats and extends along the lengths of thin filaments.

Equilibrium and velocity sedimentation data indicate that the nebulin fragments extend approximately 0.22 nm per amino acid, assuming a prolate ellipsoid as a model of shape. This length is greater than that of an α-helix, which extends 0.15 nm per amino acid. Previous studies by circular dichroism indicated that a nebulin fragment has less than 10% α-helix content in aqueous solution (*22*). Thus, the suggestion that nebulin may be induced into an α-helical conformation upon binding to actin appears to be an unnecessary assumption (*23*), since nebulin superrepeats in solution are extremely elongated even without a large composition of α-helix. Indeed, if nebulin is not localized to the central cleft of actin filaments but instead wraps around the exterior of actin, as has been proposed in our models (*7*, *22*), then nebulin would need to be longer than a simple α-helix. If a nebulin superrepeat extends such as tropomyosin winding along the outermost perimeter of actin, then it could traverse a path of at approximately 50 nm. An average nebulin superrepeat is approximately 245 amino acids in size (seven modules at 35 amino acids each); therefore, the length per amino acid to extend 50 nm is 0.20 nm/aa. These

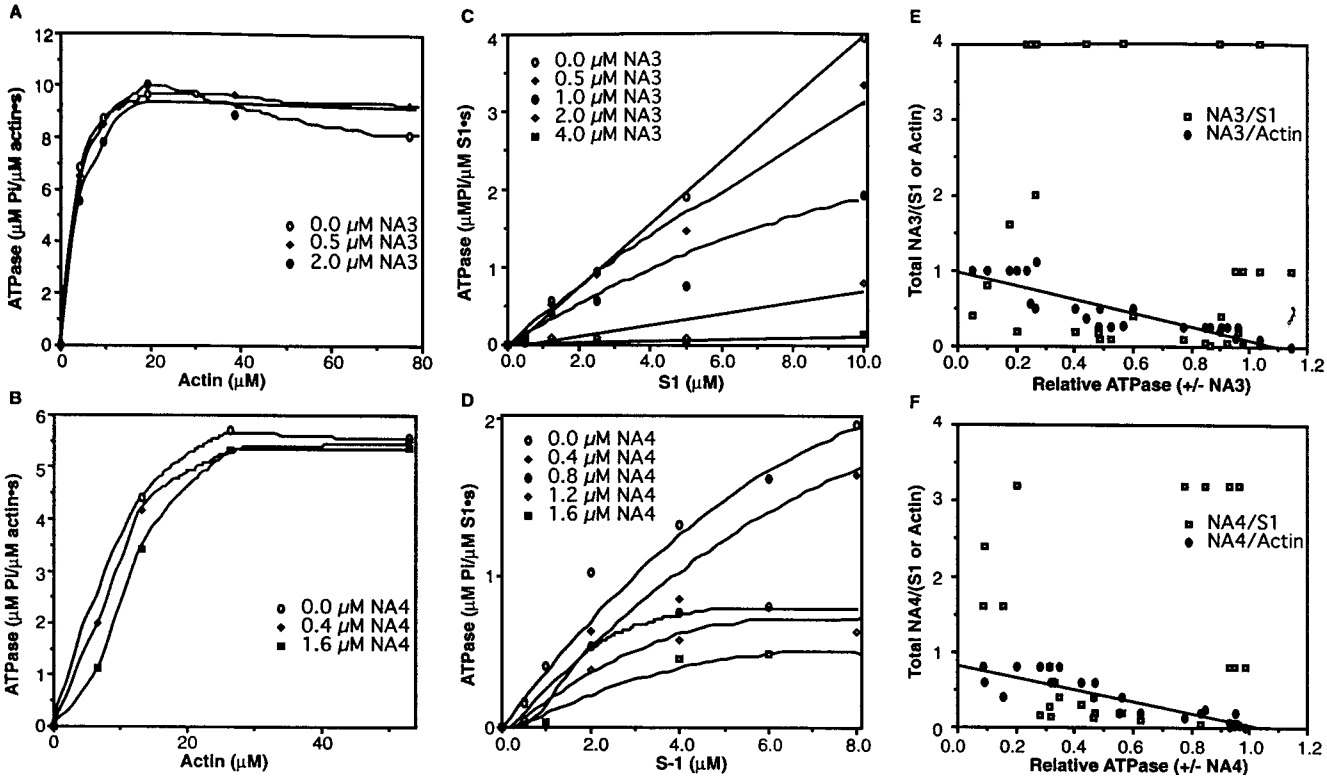

FIGURE 8: Inhibition of actin-activated ATPase activities by NA4 and NA3. Actin activation of S1 ATPase activity in 2 mM $MgCl_2$, 1 mM $CaCl_2$, and 10 mM imidazole (pH 7.0) at 25 °C is measured in the presence of varying concentrations of NA4 (0−1.6 μM) (A, C, and E) or NA3 (0−2.0 μM) (B, D, and F) by the Malachite Green method of detecting inorganic phosphate. Controls of S1 ATPase activity in the absence of actin are subtracted out to yield the actin-activated S1 ATPase activity. (A, B) Actin-activated S1 ATPase activities of varying concentrations of actin (0−80 μM) and a fixed concentration of S1 (0.5 μM). Data are fit by interpolation. (C, D) Actin-activated S1 ATPase activities of varying concentrations of S1 (0−10 μM) mixed with a fixed actin concentration (2.0 μM). Data are fit by linear regression. (E, F) Plots of relative ATPase as a function of relative ratios of NA3(NA4) to actin or S1. Relative ATPase data (from A−D) are correlated with the ratio of nebulin fragment to actin (filled circles and straight lines) but not with the ratio of nebulin fragment to S1 (highly scattered open squares). Data are fit by linear regression. Similar results for actin-activated heavy meromyosin ATPase activities are also obtained (Data not shown).

dimensions are consistent with those calculated for nebulin fragments from the centrifugation data (see Table 1) and can be explained by structures other than an α-helix such as a 3_{10} helix or some combination of β-strand, random coil, and helix.

The elongated structures of the nebulin fragment support the hypothesis that they can interact with multiple actins along a filament. It has been postulated that each of the seven modules of a superrepeat may bind to separate actin molecules. Chemically synthesized nebulin fragments of one module each bind to actin, but with very low affinity ($K_d = 10^3$ M). Nebulin superrepeats bind to actin with high affinity ($K_d = 10^6$ M); however, the stoichiometry of the interaction at high ratios of nebulin fragment to actin is about 1:1. If all seven modules of a superrepeat bind to actin with high affinity, then the expected stoichiometry would be seven actins per one nebulin superrepeat. One possibility is that only one or two modules of the superrepeat bind with high affinity to actin while other modules interact with much less affinity. In this scenario, the high-affinity binding sites would out compete the low-affinity sites at high ratios of nebulin to actin giving rise to a stoichiometry of approximately one actin per superrepeat (Figure 10A, left).

Functional assays of actin support the hypothesis that lower affinity interactions occur in addition to the high-affinity ones. The fluorescence enhancement upon nebulin-induced polymerization of pyrene actin monitors the interaction of actin monomers with nebulin fragments. As nebulin fragments induce and stabilize the polymerization of pyrene actin the fluorescence intensity increases in proportion to the fraction of actin bound by nebulin (Figure 5B). When all the actin is polymerized, only one-fourth of the actin molecules are bound with high affinity by nebulin (Figure 10A, center). This stoichiometry suggests that additional low-affinity interactions between nebulin and actin promote polymerization.

ATPase assays provide further evidence for a combination of low- and high-affinity interactions between nebulin superrepeats and actin. The nebulin fragments interfere with the ability of actin to activate S1 ATPase activity. Nebulin fragments abolish completely the actin activation of S1 ATPase by binding only between one-half and one-third of the actin with high affinity (Figure 9). One nebulin superrepeat therefore influences multiple actin molecules probably by low-affinity interactions with adjacent actins. The low-affinity interactions may be less efficient at inhibiting actin-activated ATPase than they are at inducing polymerization of actin, which could explain the difference in stoichiometry between the two types of assays. An alternative explanation is that the nebulin superrepeat may bind tightly to one actin and then induces neighboring actin molecules to a conformation that is less capable of activating ATPase (Figure 10A, right).

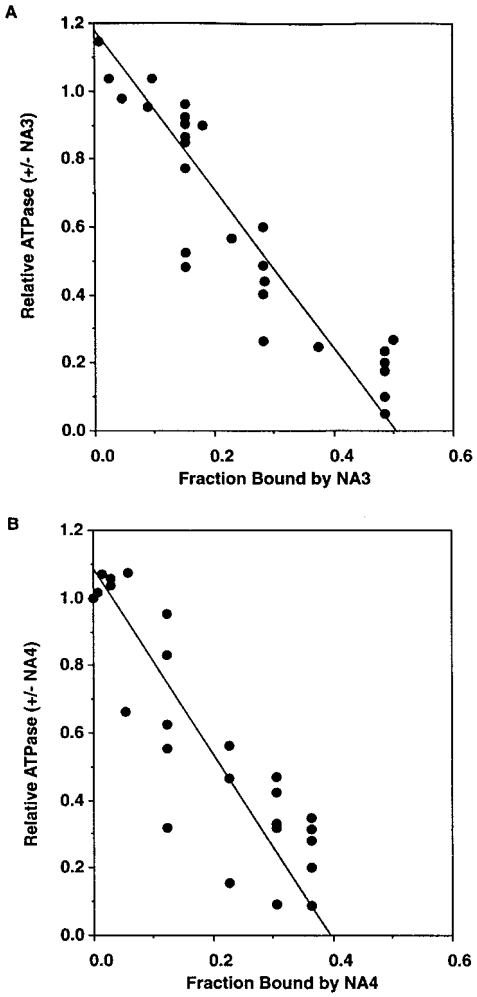

FIGURE 9: Relationship of relative actin-activated S1 ATPase activities to the fraction of actin bound by nebulin fragments. Actin-activated S1 ATPase data from Figure 8 are replotted against the fraction of actin bound by nebulin fragments (A) NA4 or (B) NA3, as calculated from binding constants from cosedimentation assays. The data are fit by linear regression.

The implications for the presence of both strong and weak binding/inhibitory sites of the superrepeat is that each superrepeat would make only a few tight contacts on the actin filaments at the strong sites, with intervening actins held in close proximity to the weaker sites. It is likely that a full length intact nebulin on the thin filament would form periodic contacts and that only regions around these strong contacts are inhibitory to ATPase activation and actomyosin association that might give rise to target regions as observed by electron microscopy (*64*).

The specific mechanism of how nebulin fragments inhibit actin activation of S1 ATPase activity is not clear. There is a correlation between the ratio of superrepeat to actin, but not S1, and actin-activated ATPase activity (Figure 8E,F). Although S1 binds with high affinity to nebulin fragments (*25*), it is unclear whether this interaction plays an important role in the ability of nebulin to inhibit actin-activated ATPase activities. One possibility is that nebulin modifies the orientation of S1 binding to actin, which interferes with binding and actin-activation (Figure 10B). Alternatively, S1 might preferentially bind in the presence of ATP to the nebulin on the actin instead of the actin itself. In the latter type of model, nebulin linking actin and S1 together could sterically prevent the approach of additional S1 molecules while keeping the nebulin-bound S1 in close proximity to the actin for enhanced reassociation (Figure 10B). A third possibility is that nebulin might prevent particular conformational changes in actin which are responsible for activation of S1 (Figure 10A, right).

The results presented here support the view that nebulin is a long polypeptide that interacts with actin at many points along its length. Nebulin is likely to have a structural role in stabilizing actin filaments as evidenced by its ability to rapidly polymerize actin (*7*). Nebulin may also play a regulatory role in actomyosin interaction, as suggested by its ability to inhibit actin activation of S1 ATPase in a dose-dependent manner. It is possible that nebulin could impose some functional diversity along the length of an otherwise homogeneous thin filament, by virtue of small differences in the sequence from one superrepeat to the next.

Nebulin's Interactions with S1 and Actin. While NA3 alters interactions between actin and S1, substantial evidence indicates that NA3 also links actin to S1 (Figure 10B). As shown previously, NA3 binds both actin and S1 with high affinities, and in the presence of ATP, S1 binding to NA3 does not affect the binding of NA3 to actin as determined by cosedimentation and ELISA binding assays (*25*). In motility assays, rhodamine phalloidin-labeled actin filaments remain tightly associated with myosin-coated coverslips in the presence of ATP and NA3, and NA3 inhibits the actin sliding over the myosin (*25*). Our present studies show that the fluorescence polarization of S1 in the presence of ATP and actin increases when NA3 is added, indicating S1 remains linked to the slowly rotating F-actin filament (Figure 2B). These observations strongly indicate that NA3 binds simultaneously to both actin and S1 in the presence of ATP (Figure 10B). It is conceivable that in the initial stage of contact of S1 with the actin−NA3 complex under strong binding conditions, S1 is held by NA3 in such an orientation that its on-rate to form strong contact with actin is greatly reduced (Figures 2 and 10B). Even in the presence of ATP, NA3 may link S1 to actin in such a way that it blocks sterically other myosin heads from approaching a critical actoS1 interface (Figure 10B), thereby interfering with both actin-activated ATPase and actin sliding over myosin during in vitro motility assays (*25*).

Implications for the Power Stroke of Actin−Myosin Cycle. The foregoing discussion of the effect of NA3 on the structure of the actoS1 strong binding complex raises the question of its relevance in the understanding of both the step-size and mechanochemical coupling efficiency of the power stroke of the actin−myosin cycle in muscle contraction. Current swinging cross-bridge theory associates the powerstroke with a bending motion in actin attached myosin heads when myosin releases its products of ATP hydrolysis. It is generally assumed that the strong binding complex of actin−S1 represents the structure and orientation of the myosin head at the end of power stroke and that the strong-binding state has been used as a reference to predict and explain the type of structural changes that are needed to cause the observed axial displacement of actin relative to myosin. The ability of nebulin to alter the orientation or structure of the strong binding complexes led us to speculate that nebulin might alter the step size of the power stroke, if it participates in the actin−myosin cycle.

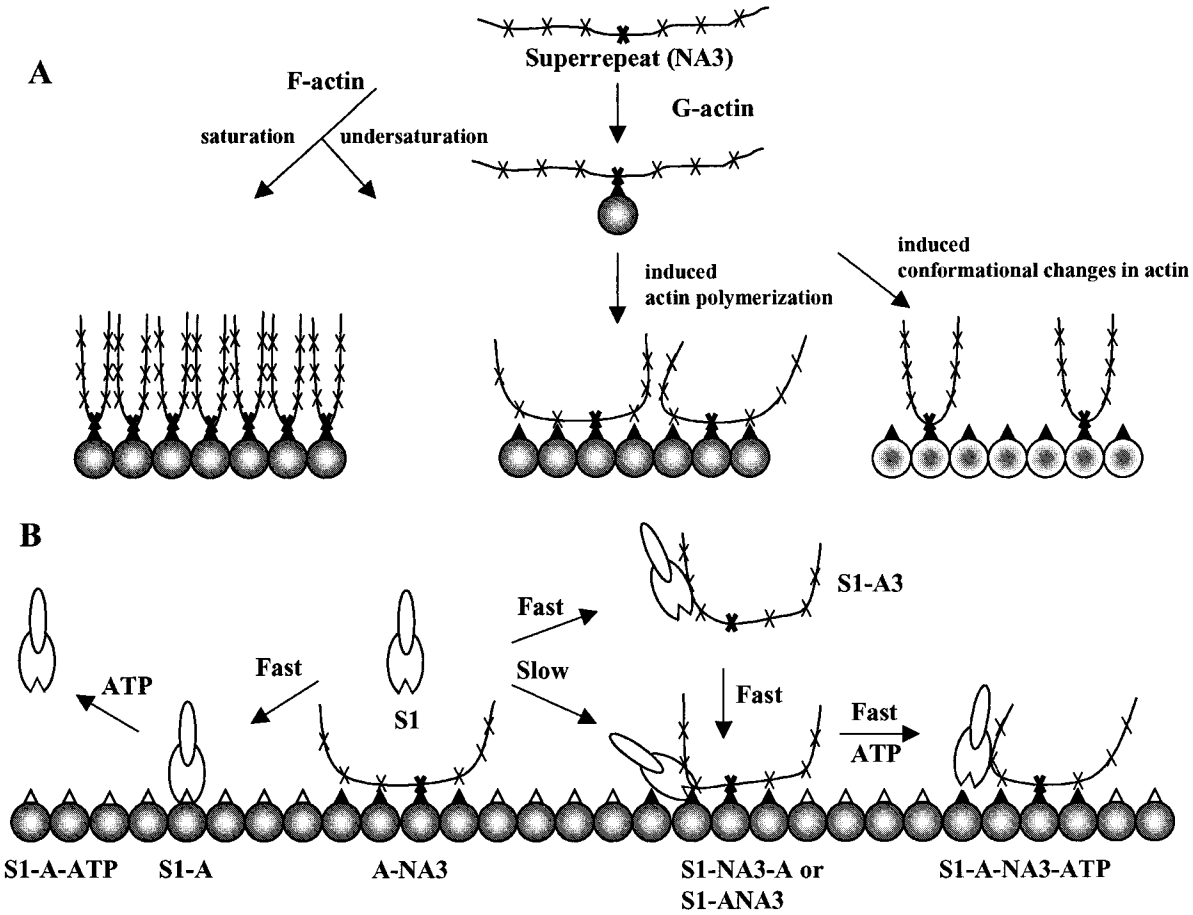

FIGURE 10: Working models of nebulin superrepeat interactions with F-actin and S1. A nebulin superrepeat is represented in black with 7 Xs representing the seven modules of the superrepeat. The bold X indicates a module with higher affinity for actin and the rest at a lower affinity. Individual actin molecules within an actin filament are illustrated by circles, and their S1 binding sites are depicted as a shaded (under the influence of nebulin) or unshaded (absence of nebulin influence) triangles. (A) The binding of nebulin superrepeat to F-actin at high ratios of superrepeat to actin (left, saturation) or low ratios of superrepeat to actin (center and right, undersaturation). At saturation, a 7:1 superrepeat to actin molar ratio, or a 1:1 module to actin ratio, would result. At under saturation, a lower ratio would result. Nebulin superrepeats accelerate actin polymerization. Two possible mechanisms are depicted: either both high- and low-affinity modules interact with adjoining actins (center) or the high-affinity module induces conformational changes of actin to facilitate polymerization (right). (B) Effect of nebulin superrepeats on actomyosin interaction. Schematic illustrations are presented for the interaction of S1 with actin (S1−A), the dissociation of actoS1 by ATP (S1−A−ATP), the inhibition of the on-rate of S1 to preformed actin/nebulin complexes (A−NA3), the binding of S1 to nebulin (S1−NA3), the binding of S1/nebulin complex to actin to form a tertiary complexes that differ significantly from the S1−A in orientation/structure (S1−NA3A or S1−A−NA3), the dissociation of the tertiary complex by ATP to form a tethered S1 on actin via nebulin (S1−A−NA3−ATP). Abbreviations are as defined in the legend of Figure 2. See the text for more discussion of the models.

Furthermore, it is conceivable that, by tethering myosin heads to actin filaments in the presence of ATP, nebulin might restrict the distance and orientation of myosin heads in the relaxed muscle and might eliminate unproductive myosin orientations during actin−myosin interaction during muscle contraction. This speculation is consistent with our observation that nebulin fragment NA3 greatly reduces the on-rate of S1 binding to actin (Figure 2). The concept that nebulin might facilitate the myosin power stroke is also suggested by our previous observations that in the presence of calcium and calmodulin, nebulin fragments cause a 50% increase in actin sliding velocities over myosin during in vitro motility assays (*25*). The decreased affinity of nebulin for actin in the presence of micromolar concentrations of calmodulin and calcium might have different consequences in vitro than in the muscle fiber, since in vitro the actin filament can be saturated with superrepeats that bind with high affinity at nearly every actin protomer, and the dissociation of some of these superrepeats could promote actin−myosin motility. In the muscle fiber where nebulin superrepeats bind strongly only periodically over every seven actin protomers, a dissociation of nebulin from actin as might be induced by high concentrations of calmodulin in the presence of calcium (*65*) could allow unproductive actomyosin interactions to occur and inhibit force development (Adhikari and Wang, unpublished observations). These observations are consistent with a role for nebulin in improving the efficiency of productive actomyosin interactions.

In summary, the nebulin fragment, NA3, which corresponds to one superrepeat of the nebulin sequence, is shown to substantially alter the binding of S1 to actin. This change in the actoS1 complex is manifested in a greatly reduced on-rate of S1 binding to actin and a profound change in the resulting actoS1 complex. These effects are largely mediated through a single strong binding site in each superrepeat that inhibits some forms of actoS1 interactions. It is tempting to speculate that this inhibitory effect might play a role in reducing suboptimal actomyosin interactions that might otherwise occur, for instance, away from recently identified target zones on the thin filament (*64*).

ACKNOWLEDGMENT

We are indebted to Dr. Boyd Hardesty for the use of his spectrofluorometer.

REFERENCES

1. Locker, R. H., and Wild, D. J. (1986) *J. Biochem. 99*, 1473−1484.
2. Wang, K., and Wright, J. (1988) *J. Cell Biol. 107*, 2199−2212.
3. Kruger, M., Wright, J., and Wang, K. (1991) *J. Cell Biol. 115*, 97−107.
4. Labeit, S., Gibson, T., Lakey, A., Leonard, K., Zeviani, M., Knight, P., Wardale, J., and Trinick, J. (1991) *FEBS Lett. 282*, 313−316.
5. Maruyama, K., Matsuno, A., Higuchi, H., Shimaoka, S., Kimura, S., and Shimizu, T. (1989) *J. Muscle Res. Cell Motil. 10*, 350−359.
6. Pierobon-Bormioli, S., Betto, R., and Salviati, G. (1989) *J. Muscle Res. Cell Motil. 10*, 446−456.
7. Jin, J., P., and Wang, K. (1991) *J. Biol. Chem. 266*, 21215−21223.
8. Wright, J., Huang, Q. Q., and Wang, K. (1993) *J. Muscle Res. Cell Motil. 14*, 476−483.
9. Wang, K., Knipfer, M., Huang, Q. Q., van Heerden, A., Hsu, L. C., Gutierrez, G., Quian, X. L. and Stedman, H. (1996) *J. Biol. Chem. 271*, 4304−4114.
10. Labeit, S., and Kolmerer, B. (1995) *J. Mol. Biol. 248*, 308−315.
11. Millevoi, S., Trombitas, K., Kolmerer, B., Kostin, S., Schaper, J., Pelin, K., Granzier, H. and Labeit, S. (1998) *J. Mol. Biol. 282*, 111−123.
12. Gonsior, S. M., Gautel, M. and Hinssen, H. (1998) *J. Muscle Res. Cell Motil. 19*, 225−235.
13. Moncman, C. L., and Wang, K. (1995) *Cell Motil. Cytoskeleton 32*, 205−225.
14. Moncman, C. L., and Wang, K. (2000) *J. Muscle Res. Cell Motil. 21*, 153−169.
15. Politou, A. S., Millevoi, S., Gautel, M., Kolmerer, B., and Pastore, A. (1998) *J. Mol. Biol. 276*, 189−202.
16. Pfuhl, M., Winder, S. J., Castiglione Morelli, M. A., Labeit, S., and Pastore, A. (1996) *J. Mol. Biol. 257*, 367−384.
17. Shih, C.-L., Chen, M.-J. G., and Wang, K. (1997) *Biochemistry 36*, 1814−1825.
18. Zhang, J. Q., Weisberg, A., and Horowits, R. (1998) *Biophys. J. 74*, 349−59.
19. Moncman, C. L., and Wang, K. (1994) *Mol. Biol. Cell 5*, 516a.
20. Jin, J.-P., and Wang, K. (1991) *FEBS Lett. 281*, 93−96.
21. Tatsumi, R., Hattori, A., and Takahashi, K. (1993) *J. Biochem. 113*, 797−804.
22. Chen, M.-J. G., and Wang, K. (1994) *Arch. Biochem. Biophys. 310*, 310−317.
23. Pfuhl, M., Winder, S. J., and Pastore. A. (1994) *EMBO J. 13*, 1782−1789.
24. Chen, M.-J. G., Shih, C.-L., and Wang, K. (1993) *J. Biol. Chem. 268*, 20327−20334.
25. Root, D. D., and Wang, K. (1994) *Biochemistry 33*, 12581−12591.
26. Matsumura, F., and Yamashiro, S. (1993) *Curr. Opin. Cell Biol. 5*, 70−76.
27. Spudich, J. A., and Watt, S. (1971) *J. Biol. Chem. 246*, 4866−4871.
28. Godfrey, J. E., and Harrington, W. F. (1970) *Biochemistry 9*, 886−893.
29. Weeds, A., and Pope, B. (1977) *J. Mol. Biol. 111*, 129−157.
30. West, J. J., Nagy, B., and Gergely, J. (1967) *J. Biol. Chem. 242*, 1140−1145.
31. Gill, S. C., and von Hippel, P. H. (1989) *Anal. Biochem. 182*, 319−326.
32. Cooper, J. A., Walker, S. B., and Pollard, T. D. (1983) *J. Muscle Res. Cell Motil. 4*, 253−262.
33. Cheung, H. C., and Liu, B. (1984) *J. Muscle Res. Cell Motil. 5*, 65−80.
34. Cheung, H. C., Gonsoulin, F., and Garland, F. (1983) *J. Biol. Chem. 258*, 5775−5786.
35. Scott, T. A., Spencer, R. D., Leonard, N. J., and Weber, G. (1970) *J. Am. Chem. Soc. 92*, 687−695.
36. Kielley, W. W., and Bradley, L. B. (1956) *J. Biol. Chem. 218*, 653−659.
37. Baykov, A. A., Evtushenko, O. A., and Avaeva., S. M. (1988) *Anal. Biochem. 171*, 266−270.
38. Steiner, R. F. (1991) in *Topics in fluorescence spectroscopy* (Lakowicz, J. R., Ed.) pp 1−52, Plenum Press, New York.
39. dos Remedios, C. G., Miki, M., and Barden, J. A. (1987) *J. Muscle Res. Cell Motil. 8*, 97−117.
40. Dale, R. E., Eisinger, J., and Blumberg, W. E. (1979) *Biophys. J. 26*, 161−194.
41. Trayer, H. R., and Trayer, I. P. (1983) *Eur. J. Biochem. 135*, 47−59.
42. Hudson, E. N., and Weber, G. (1973) *Biochemistry 12*, 4154−4161.
43. Van Holde, K. E., and Baldwin, R. L. (1958) *J. Phys. Chem. 62*, 734−743.
44. Laemmli, U. K. (1970) *Nature 227*, 680−685.
45. Root, D. D., and Wang, K. (1996) in *The Protein Protocols Handbook* (Walker, J. M., Ed.) pp 39−43, Humana Press Inc., Totowa, NJ.
46. Lin, J. J.-C. (1981) *Proc. Natl. Acad. Sci. U.S.A. 78*, 2335−2339.
47. Kouyama, T., and Mihashi. K. (1980) *Eur. J. Biochem. 114*, 33−38.
48. McKillop, D. F. A., and Geeves, M. A. (1991) *Biochem. J. 279*, 711−718.
49. Greene, L. E. (1981) *Biochemistry 20*, 2120−2126.
50. Taylor, E. W. (1991) *J. Biol. Chem. 266*, 294−302.
51. Burke, M., and Reisler, E. (1977). *Biochemistry 16*, 5559−5563.
52. Wells, J. A., and Yount, R. G. (1982) *Methods Enzymol. 85*, 93−116.
53. Crosbie, R. H., Chalovich, J. M., and Reisler, E. (1992) *Biochem. Biophys. Res. Commun. 184*, 239−245.
54. Miki, M., and Wahl, P. (1984) *Biochim. Biophys. Acta 790*, 275−283.
55. Botts, J., Thomason, J. F., and Morales, M. F. (1989) *Proc. Natl. Acad. Sci. U.S.A. 86*, 2204−2208.
56. Rayment, I., Holden, H. M., Whittaker, M., Yohn, C. B., Lorenz, M., Holmes, K. C., and Milligan. R. A. (1993) *Science 261*, 58−65.
57. Rayment, I., Rypniewski, W. R., Schmidt-Base, K., Smith, R., Tomchick, D. R., Benning, M. M., Winkelmann, D. A., Wesenberg, G., and Holden, H. M. (1993) *Science 261*, 50−58.
58. Lorenz, M., Popp, D., and Holmes, K. (1993) *J. Mol. Biol. 234*, 826−836.
59. Holmes, K. C., Popp, D., Gebhard, W., and Kabsch, W. (1990) *Nature 347*, 44−49.
60. Baudet-Nessler, S., Jullien, M., Crosio, M. P., and Janin, J. (1993) *Biochemistry 32*, 8457−8464.
61. Cheung, H. C. (1991) in *Topics in fluorescence spectroscopy* (Lakowicz, J. R., Ed.) pp 127−176, Plenum Press, New York.
62. Ajtai, K., and Burghardt, T. P. (1987) *Biochemistry 26*, 4517−4523.
63. Cantor, C. R., and Schimmel, P. R. (1980) in *Biophysical chemistry, part II*: *Techniques for the study of biological structure and function*. W. H. Freeman and Company, New York.
64. Taylor, K. A., Schmitz, H., Reedy, M. C., Goldman, Y. E., Franzini-Armstrong, C., Sasaki, H., Tregear, R. T., Poole, K., Lucaveche, C., Edwards, R. J., Chen, L. F., Winkler, H., and Reedy, M. K. (2000) *Cell 99*, 421−431.
65. Ao, X., and Lehrer, S. S. (1995) *J. Cell Sci. 108*, 3397−3403.

BI0015010